Acquisition and Control of a Precision Formation Flying Mission

by

John M. Field

S.B., Aerospace Engineering
Massachusetts Institute of Technology, 2008

Submitted to the Department of Aeronautics and Astronautics
in partial fulfillment of the requirements for the degree of

Master of Science in Aeronautics and Astronautics

at the

MASSACHUSETTS INSTITUTE OF TECHNOLOGY

June 2010

Author .....
Department of Aeronautics and Astronautics
May 21, 2010

Certified by .....
David W. Miller
Professor of Aeronautics and Astronautics
Thesis Supervisor

Certified by .....
Alvar Saenz-Otero
Research Scientist, Aeronautics and Astronautics
Thesis Supervisor

Accepted by .....
Eytan H. Modiano
Associate Professor of Aeronautics and Astronautics
Chair, Committee on Graduate Students

Acquisition and Control of a Precision Formation Flying Mission

by

John M. Field

Submitted to the Department of Aeronautics and Astronautics
on May 21, 2010, in partial fulfillment of the
requirements for the degree of
Master of Science in Aeronautics and Astronautics

Abstract

Using formation flying spacecraft as space-based interferometers will provide images of unprecedented resolution. Missions such as Stellar Imager plan to use multiple spacecraft in a formation instead of a typical monolithic space telescope, achieving a resolution up to 0.1 milliarcseconds. In order to assemble into a formation, these satellites must first locate each other using limited field-of-view sensors. Once the satellites are in a formation, the path length of the light going to the combiner satellite must be controlled to nanometer levels to produce an image of high quality. One solution to control to such precision is to use staged control methods, utilizing multiple actuators with overlapping strokes and bandwidths.

This thesis first provides an algorithm for three satellites to initialize into a formation using relative measurements and limited field-of-view sensors. The satellites perform a search to locate each other, accurately point their transmitters at each other, and move into an equilateral triangle formation.

This thesis also provides the framework for developing a staged pointing and phasing testbed using the Synchronized Position Hold Engage Reorient Experimental Satellites (SPHERES) as the coarse stage. The pointing actuation is provided by a fast steering mirror and a linear stage, and the phasing actuation is provided by an optical delay line consisting of a voice coil mirror and a piezo mirror.

Thesis Supervisor: David W. Miller
Title: Professor of Aeronautics and Astronautics

Thesis Supervisor: Alvar Saenz-Otero
Title: Research Scientist, Aeronautics and Astronautics

Acknowledgments

I would like to first thank Prof. David W. Miller for the opportunity to work in the Space Systems Lab and the chance to develop tests that ran inside the ISS. I would like to thank Dr. Alvar Saenz-Otero for all his help throughout my time at MIT. Without him I'm sure my MIT experience would have been lacking. I would like to thank the members of the SSL and the SPHERES team, especially Jacob Katz, Christophe Mandy, and Brent Tweddle for their advice and assistance whenever I needed it. I would like to thank Paul Bauer for his help with the electronic aspects of SIMO as well. I would also like to thank NASA-Goddard and Aurora Flight Sciences for their support of the SIMO project. Finally, I would like to thank my family and Brooke for their support.

Contents

List of Figures

List of Tables

Chapter 1

Introduction

1.1 Motivation

Formation flying spacecraft will expand the possibilities of scientific achievements in space. Several missions have been proposed for formation flying spacecraft, including space-based interferometers. Space-based interferometers on formation flying satellites will allow for large baseline interferometry, allowing us to see farther into the depths of the universe, at unprecedented resolution.

There are many challenges that the formation flying spacecraft must face during a mission. One of the first is during deployment. After being deployed, the satellites must use relative navigation to locate each other and assemble into their desired formation. In order to complete this, the satellites must search for each other and then perform maneuvers using relative position information.

During a formation flying interferometry mission, the relative position between the satellites must be controlled precisely. It is essential that the path length of the light that is being interfered is controlled on the order of nanometers. Without high-precision control, the resulting image will not be of high quality. The satellites themselves are not capable of high enough precision control to achieve a high-quality image. Therefore, multiple stages are employed with overlapping strokes and bandwidths to reach the desired precision.

Formation flying interferometers are being developed to surpass the quality of im-

ages produced by current technology. The Hubble Space Telescope (HST), launched in 1990, has captured the most detailed visible-light images to date.The HST operates mainly in the visible and ultra-violet spectrum and is capable of an angular resolution on the order of 0.03 arcseconds [6]. The James Webb Space Telescope (JWST), which is scheduled for launch in 2014, is planned to succeed the Hubble telescope. The JWST will operate mainly in the infrared spectrum with an angular resolution on the order of 0.1 arcseconds, operating at Earth-Sun L2. [21]

The Stellar Imager (SI) mission will be designed to achieve an angular resolution of 0.1 milliarcseconds. SI's science focuses on the role of magnetism in the universe, particularly on magnetic activity on the surfaces of stars like the Sun. SI will enable detailed study of magnetic processes and their roles in the origin and evolution of structure and in the transport of matter throughout the universe. SI will focus on the ultra-violet and visible spectrum, and will produce images with hundreds of times more detail than Hubble. SI will bring the study of dynamical evolution of many astrophysical objects into reach: hours to weeks between successive images will detect dramatic changes in many objects, e.g., mass transfer in binaries, pulsation-driven surface brightness variation and convective cell structure in giants and supergiants, jet formation and propagation in young planetary systems, reverberating active galactic nuclei, and many others. [4]

A concept image for Stellar Imager can be seen in Figure 1-1. Stellar Imager will consist of up to 30 spacecraft with 1-2 m diameter mirrors, as well as a combiner spacecraft, in Earth-Sun L2 orbit. The spacecraft will be separated by 100-1000 m, and together they will form a Fizeau interferometer, gathering information about the sun as well as other similar stars. In order to create a high quality image, the relative position between the spacecraft must be controlled to high precision and accuracy. The spacecraft themselves must be controlled to mm-cm levels, and the optical surfaces must be controlled to nm-μm levels. [4]

Several other proposed mission include formation flight and interferometry. The Terrestrial Planet Finder Interferometer (TPF-I) mission, seen in Figure 1-2, consists of four 4 m infrared telescopes and one combiner spacecraft. TPF-I will search for

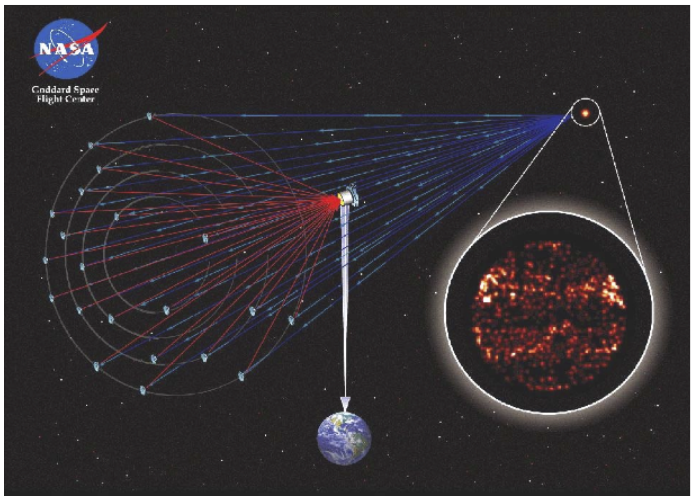

Figure 1-1: Concept for Stellar Imager [4]

habitable planets around nearby stars and will also look for signs of life on those planets.[20] The Laser Interferometer Space Antenna (LISA) will observe astrophysical and cosmological sources of gravitational waves using a three spacecraft triangular formation. LISA will act as a Michelson interferometer with equal arms of 5 million km.[19]

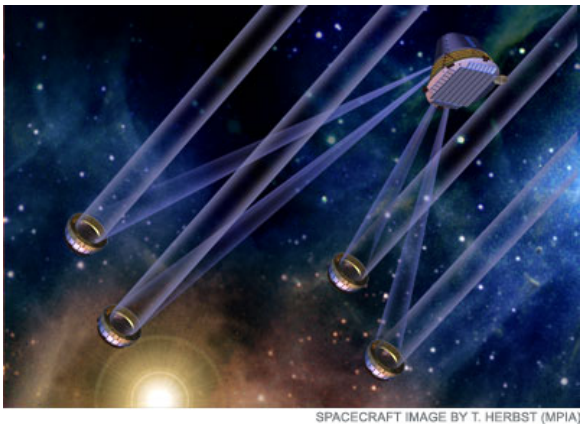

Figure 1-2: Terrestrial Planet Finder Interferometer mission concept [20]

1.2 Background

1.2.1 Formation Acquisition

The problem of formation initialization (FI) is the process of using limited field-of-view on-board sensors to establish communications among the formation members and to acquire the relative positions and velocities of a set of distributed spacecraft [8]. Scharf and others at JPL developed and algorithm which guarantees spatial initialization for N-spacecraft formations [29].

In the algorithm, the satellites have a limited field of view sensor, and two satellites must have a simultaneous "front-to-front lock" (see Figure 1-3) in order for communications and relative sensing to be possible. The algorithm guarantees initialization for an N-spacecraft formation. Three different searches are developed in order to ensure initialization: an in-plane search, an out-of-plane search, and a near-field search. The problem of initializing N spacecraft is also reduced to a problem of joining a set of multi-spacecraft sub-formations.

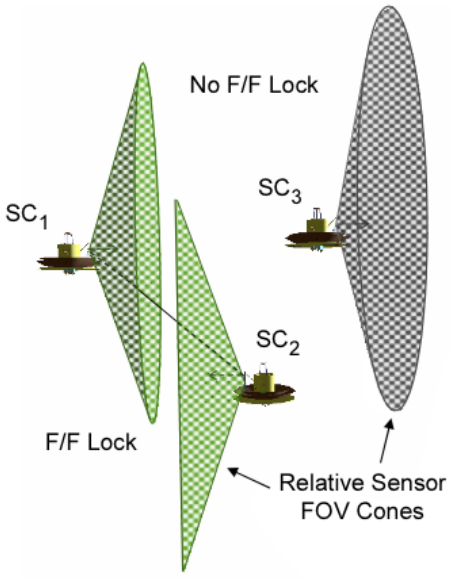

Figure 1-3: SC_1 and SC_2 have a front-to-front lock, SC_3 has no front-to-front lock [29]

A 150000 case Monte-Carlo simulation of a two-spacecraft formation was run, us-

ing different initializations while accounting for realistic mission constraints, including limited sensor field-of-view (FOV) and sun-angle restrictions. The analysis showed that all cases were able to achieve the front-to-front lock.

Hardware testing of a formation initialization algorithm has been performed by Sakamoto [18] [16]. Several tests were run using the SPHERES satellites, both in 3 degrees of freedom (DOF) and 6 DOF. The tests were run with limited FOV transmitters, omnidirectional receivers, and omnidirectional communication. Upon completion of the work, two satellites were able to locate each other and point their beacon faces towards each other. The tests followed the following four steps:

1. The Master satellite[1] searches for the other satellite through a prescribed rotation.

2. The Follower satellite notifies the Master of reception of ultrasound (U/S) signal using direct satellite-to-satellite communication.

3. The Follower satellite starts the state estimation using the U/S signal emitted from the Master, and then points its beacon-transmitter face toward the Master according to the estimated states.

4. Once the Master receives the U/S signal emitted from the Follower, the Master also estimates its states relative to the Follower, and then points its beacon-transmitter face toward the Follower.

The work in this thesis in Chapter 2 expands upon the work performed by Sakamoto to a three satellite formation.

1.2.2 Interferometry Testbeds

NASA has developed the Fizeau Interferometry Testbed (FIT) in support of Stellar Imager, as well as other missions that will require Fizeau interferometry. FIT is being used to study wavefront sensing and control, which will be essential for SI,

[1]The Master and Follower satellites were defined before the start of the test

in a ground testbed. The testbed consists of several actuated mirrors (7 mirrors as of August, 2007, with plans to increase to 18, then 30) in a Golay pattern. The objective is to sense and control the wavefront by actuating the mirrors, achieving a phased image. [15] The goal of the Synthetic Imaging Maneuver Optimization (SIMO) testbed, discussed in Chapter 3, is to combine precise control, similar to the FIT, with the coarse control already demonstrated by the SPHERES satellties.

Several other interferometry testbeds have been developed or are planned, both terrestrial and in space. The W.M. Keck Observatory combines two 10 m telescopes with an 85 m baseline to form an interferometer capable of 5 milliarcsecond resolution at 2.2 μm[5]. The Space Interferometry Mission Lite will consist of a single spacecraft with a 6 m baseline Michelson interferometer[10].

1.2.3 Staged Control

One of the keys to formation flying interferometry missions is staged control. If there were a single actuator that had large stroke, high bandwidth, and high resolution, staged control would not be necessary. However, actuators that have a large stroke tend to have lower bandwidth and resolution, whereas actuators with high bandwidth and resolution tend to have a smaller stroke. Staged control allows a system to have large stroke, high bandwidth, and high resolution. The satellite is generally not capable of precise enough control on its own for interferometry missions, where the control of the path length of the incoming light must be accurate to fractions of a wavelength. It is therefore necessary to add intermediate stages, with overlapping strokes and bandwidths. There has been some work previously on using staged control for interferometric missions. In [13], the author evaluates how actuator capabilities and constraints affect the system performance using Lyapunov and stochastic linearization methods.

In [12], the author discusses the development of a staged pointing payload for the SPHERES satellites. In this payload, the SPHERES satellite travels to a desired location, and a fast steering mirror attempts to point a laser beam (also attached to the satellite) towards a retroreflector. The Synthetic Imaging Maneuver Optimization

(SIMO) testbed, discussed in Chapter 3, instead uses an off-board laser beam which it must first locate. A fast steering mirror is then used to reflect the beam towards a sensor. This is representative of a spacecraft that must position it self within a formation and reflect light from a star or other light source towards a combiner spacecraft.

In [27], a testbed for investigating control techniques for a separated spacecraft interferometer was developed. The ground testbed consisted of coarse control by free-flying vehicles on a granite table top and a fine stage which pointed a laser at a target.

There have also been several studies on using optical delay lines to control the path length of a beam. This includes developing an nanometer level optical delay line control law[7], as well as a nonlinear control law[9][14].

1.3 SPHERES Testbed

Both the Formation Acquisition and Staged Pointing and Phasing portions of this thesis are dependent on the Synchronized Position Hold Engage Reorient Experimental Satellites (SPHERES) testbed. The following is a background on the testbed.

1.3.1 Overview

The SPHERES testbed provides a low-cost, risk-tolerant environment to demonstrate and validate metrology, control, and autonomy algorithms. There are two main testbed locations: 6 degrees of freedom (DOF) in microgravity onboard the International Space Station (ISS), and 3 DOF flat table testing in the MIT Space Systems Laboratory (SSL). Both testbeds have access to three SPHERES satellites, seen in Figure 1-4. The testbed consists of three satellites, five ultrasonic beacons, and a laptop computer for starting tests and downloading data. The satellites have all of the necessary modules onboard, and are autonomous.

Each satellite contains the following components:

- Power: two rechargeable battery packs.
- Propulsion: 12 cold-gas thrusters are positioned about the satellite and a tank of CO_2 provides propellant.
- Computing: an onboard Texas Instruments C6701 DSP runs the program developed by the scientist and an FPGA samples and digitizes the sensor signals.
- Communications: two radio-frequency channels are used for inter-satellite communication, as well as for communication with the laptop.
- Position and Attitude Determination System (PADS): Each satellite has 24 onboard ultrasound receivers, which receive ultrasound signals from five ultrasound transmitters (also called beacons) positioned at known locations on the edges of the test volume. Each satellite also has onboard gyroscopes and accelerometers.

More in-depth information can be found in [11] and [28].

Figure 1-4: SPHERES satellite[17]

1.3.2 Metrology

The SPHERES metrology system provides the measurements necessary for the satellite to estimate its position, velocity, attitude, and angular rate. Five ultrasound beacons are positioned in known locations about the frame of the testing location. To instruct the beacons to emit their ultrasound chirp, one satellite sends an infrared signal, which the beacons receive. Upon receiving the infrared, each beacon sends

an ultrasound chirp at a predefined time after receiving the infrared. Twenty-four ultrasound receivers are positioned around the shell of the satellite, and they receive the ultrasound chirps. Time of flight measurements are recorded from the beacon transmitters to the receivers, and these measurements, along with the known locations of the beacon transmitters, are used to estimate the satellite's position, velocity, attitude, and rotation rate. The satellite also has internal gyroscopes which are used to add more measurements to aid in estimating attitude and rotation rate.

Each satellite also has a transmitter beacon located on its body -X face. This transmitter can be used estimate relative range and range rates between two satellites in the absence of the global positioning beacons. Chapter 2 describes formation acquisition techniques, which use this onboard beacon.

1.3.3 Expansion Port

Each SPHERES satellite has an expansion port on its body +X face. The port consists of a 100 pin connector that can provide power to and transfer data to/from an expansion item. The expansion port has an RS-232 UART connection, which is used in the SIMO payload, discussed in Chapter 3. There are four 2-56 attachment points as well, making it possible to physically mount an expansion item to the satellite. A picture of the expansion port can be seen in Figure 1-5.

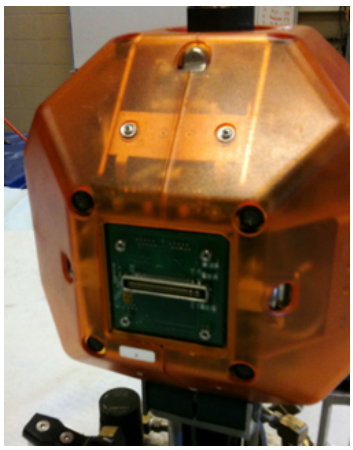

Figure 1-5: SPHERES expansion port

1.3.4 External Stack

The SPHERES external stack will be used to aid in communications in the SIMO testbed. The external stack is a SPHERES satellite that is only capable of performing processing and communications tasks. It is also capable of interfacing with other payloads through an expansion port. The stack can be seen below in Figure 1-6.

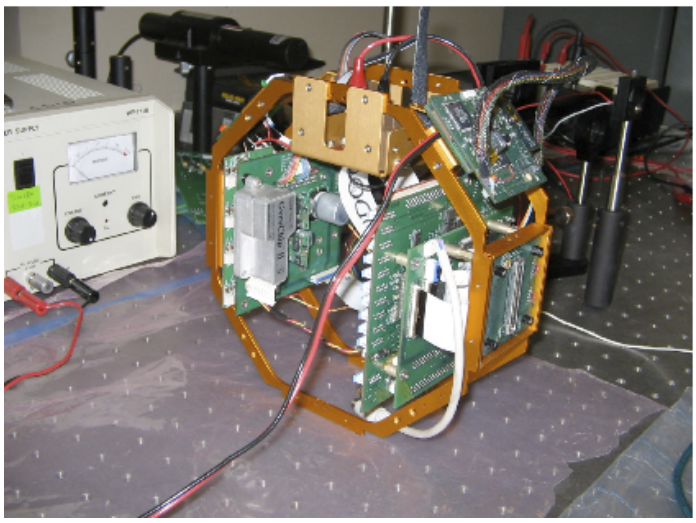

Figure 1-6: SPHERES External Stack

1.4 Thesis Objectives

- To develop and test on hardware an algorithm for three satellite formation acquisition.
- To develop a testbed for staged pointing and phasing control and test the validity of the testbed.

1.5 Thesis Outline

- Chapter 2 discusses an algorithm for three satellite formation acquisition using relative measurements with limited field-of-view sensors.

- Chapter 3 discusses the hardware and control elements for the SIMO payload, which uses staged pointing and phasing to enable interference, with relevance towards space-based interferometers.
- Chapter 4 provides the results from the formation acquisition tests, as well as the results from the development of the SIMO payload.
- Chapter 5 summarizes the work presented in Chapters 2 through 4 and offers concepts for future work.

Chapter 2

Formation Acquisition: "Lost in Space"

When formation flying satellites are deployed, the satellites must first locate each other in order to create a formation. The satellites will often have limited field-of-view (FOV) sensors, so the satellites must perform a search maneuver in order to find each other. The satellites then use relative measurements to move into the desired configuration. If there is a failure at some point during the mission, the satellites may also need to re-initialize the formation, again performing the search and relative ranging maneuvers.

A three satellite "Lost in Space" algorithm was demonstrated using the SPHERES testbed. The three satellite algorithm was developed by expanding on the two satellite work performed by Sakamoto, which also used the SPHERES satellites [16] [18]. Tests were run in simulation, on the ground in the Space Systems Lab, and onboard the International Space Station to validate the algorithm. The problem statement and the development of the algorithm follow in this chapter, while the results from testing are detailed in Chapter 4.

2.1 Overview

For formation flying satellites, if no high-accuracy terrestrial navigation aids like GPS are available, the satellites will be required to create a formation using only relative position measurements, though the global attitude knowledge may be obtained using a sensor such as a star tracker. The initial formation capturing procedure consists of the following four stages, as defined by Sakamoto [16]:

1. The multiple satellites are deployed without *a priori* knowledge of the other satellites positions ("lost in space"), emulating a release from a launch vehicle or a case of contingency.

2. The satellites capture the other satellites within their relative sensor range, which typically has a limited field-of-view (FOV).

3. The satellites null their range rates.

4. The satellites position themselves within an array.

The sequence must be performed using only the known relative position measurements and global attitude data. Often a satellite's sensors have limited fields of view, meaning that the satellite will have to perform a search maneuver to locate the other satellites in the formation.

The SPHERES satellites, for example, have an onboard ultrasound (U/S) transmitter that can be used for relative navigation. The transmitter has an FOV of approximately 60°. The satellites are capable of omnidirectional reception of the transmitted U/S signal, using the 24 U/S receivers that are distributed on the outer shell of the satellite. The SPHERES satellites are capable of omnidirectional communication as well.

During the initial set of tests, the satellites used the onboard transmitter for performing relative measurements. However, the tests showed that the FOV of the transmitter was larger than expected, and there were also issues with the ultrasound signal reflecting off of surfaces during the test. So, the next set of tests used a

simulated onboard transmitter. The satellites communicated their global states and attitudes to each other and determined which satellites they could "see" based on the position and attitude of the other satellites. The simulated transmitter that was used was given the same specifications as the SPHERES onboard transmitter: a FOV of 60°located on the -X face of the satellite.

Using a simulated transmitter makes it simple to alter the transmitter/receiver configuration. The FOV of the transmitter can be changed, the transmitter could be moved to a different face, and the receiver could be configured to also have a limited FOV. This makes it possible to change the configuration to represent a satellite that is planned to be used in a specific mission.

The three satellites begin in an unknown configuration, and the desire is to have the three satellites form an equilateral triangle with each satellite pointing it's transmitter at another satellite, and no satellites pointing at each other. With three satellites, this formation ensures that the field of view of each satellite will constantly be received by another satellite. An equilateral triangle is a simple formation that should be easy for the satellites to achieve and will limit collisions. An equilateral triangle, or Golay-3 formation, is also the optimal formation for compactness for three satellites. A compact formation can lead to full u-v coverage with small apertures. [18] A possible starting configuration and a possible final configuration can be seen in Figure 2-1.

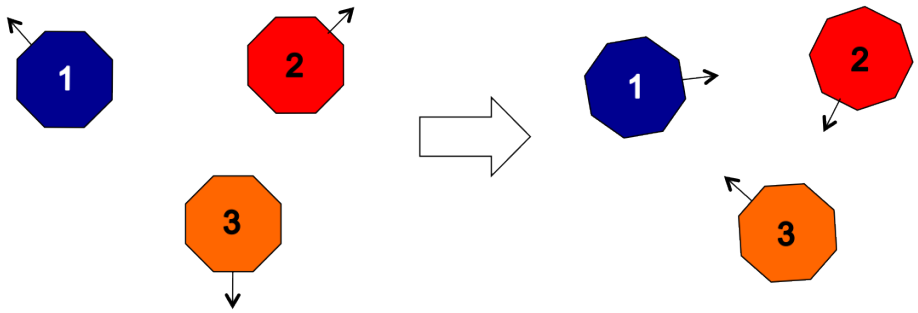

Figure 2-1: Possible starting configuration and desired final configuration

2.2 Method

The satellites follow the following steps, which are described in further detail in the succeeding sections. Figure 2-2 shows an example of how the formation may look at each step. The actual progression will vary, depending on the order in which the satellites locate themselves.

1. Each satellite performs a three-dimensional search maneuver (a "peal") until either the satellites transmitter is detected by another satellite, or the pealing satellite detects a transmission from another satellite. The two satellites that first locate each other become "partners." (Figure 2-2a)

2. Step two consists of two simultaneous parts:

   (a) The two satellites that are partners point their transmitter faces towards each other using the relative measurements. The satellites null their range rates with respect to each other.

   (b) The third satellite partners with the first satellite it detects (or is detected by) and points its transmitter face at that satellite. The third satellite also nulls its range rates with respect to its partner.

   The satellite that has two satellites pointing at it is now called the "Primary" satellite, the primary satellite's partner is now called "Secondary," and the third satellite is called "Tertiary." (Figure 2-2b)

3. Once the errors are low, the Secondary satellite rotates and points its transmitter at the Tertiary satellite. (Figure 2-2c)

4. The satellites move into an equilateral triangle formation by having the Secondary and Tertiary satellites move relative to the primary satellite. (Figure 2-2d)

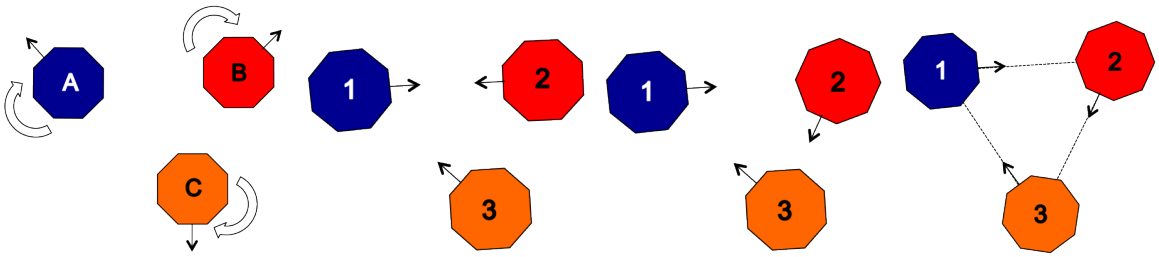

(a) Step 1 (b) Step 2 (c) Step 3 (d) Step 4

Figure 2-2: Possible progression of the initialization of a three satellite formation

2.2.1 Communication

In order to complete the maneuver, the satellites must communicate with each other. Each satellite sends out a packet of information each control period (one second) containing the following information:

- Global position (Used for calculating relative position when another satellite's transmitter is in view)
- Global velocity (Used for calculating relative velocity when another satellite's transmitter is in view)
- Direction of -X face (face on which the transmitter is located) in the global frame (used for determining when a satellite can "see" another satellite's transmitter)
- Which satellites it can currently "see"
- Time at which it first detected each other satellite
- Which satellite it is partnered with

2.2.2 Pealing Maneuver

All satellites begin by performing a "pealing" maneuver. In the maneuver, the satellite performs a three dimensional rotation so that the field of view of the transmitter covers the entire three dimensional space. Starting at its initial attitude, the satellite

performs a constant rotation about its body Z axis at $\pi/10$ rad/s while simultaneously rotating about its body Y axis at $\pi/60$ rad/s. This maneuver was also used by Sakamoto in [16] and [18]. The rates are such that the cone formed by the satellite's transmitter will cover the entire three dimensional space during the maneuver. Adjusting the rates affects how much of the space is covered by the transmitter. If the Y rotation rate is too high for a given Z rotation rate and transmitter FOV, the cone may not cover the entire space. If either of the rotation rates are too high, the satellite may not be able to accurately track the desired rotation.

The computation required for the satellite to determine it's desired attitude is shown in Equation 2.1. C_{ref} is a matrix representing the satellite's initial attitude, ω_z is the rotation rate about the body Z axis, ω_y is the rotation rate about the body Y axis, and t is the time since the start of the peal. The resulting direction cosine matrix is then converted to a quaternion and set as the target attitude for the satellite. The corresponding body rotation rates are calculated and set as targets as well.

$$DCM = \begin{pmatrix} \cos\omega_z t & \sin\omega_z t & 0 \\ -\sin\omega_z t & \cos\omega_z t & 0 \\ 0 & 0 & 1 \end{pmatrix} \begin{pmatrix} \cos\omega_y t & 0 & -\sin\omega_y t \\ 0 & 1 & 0 \\ \sin\omega_y t & 0 & \cos\omega_y t \end{pmatrix} C_{ref} \tag{2.1}$$

2.2.3 Detection

As the satellites are rotating, their beacon transmitters will be seen by the other satellites. The satellites must be able to detect when they can see another satellite's transmitter. Figure 2-3 illustrates the relationship of the satellites near detection. Satellite i can "see" satellite j's transmitter when the vector from i to j (x_i) is inside the cone made by satellite j's transmitter (d_j). Equation 2.2 describes this relationship, where θ_{FOV} is the field-of-view of the transmitter.

$$\hat{d_j} \cdot -\hat{x_i} > \cos\theta_{FOV} \tag{2.2}$$

In order to ensure that the transmitter that the satellite is seeing is valid, the

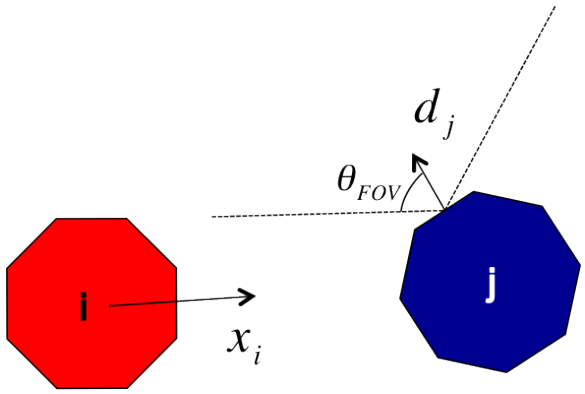

Figure 2-3: Satellites are near detection

satellite waits one control period before moving to the pointing stage. If by that time the other satellite is no longer visible, then the satellite will continue searching. This ensures that the satellite is not too close to the edge of the other satellite's transmitter cone.

If the satellites are no longer able to see each other at some point during a future maneuver, the satellites will revert to the pealing maneuver and re-partner. This could happen if there are large relative velocities between the satellites.

2.2.4 Point to Target and Null Range Rates

If a satellite receives a transmission from another satellite's beacon transmitter, it communicates with the transmitting satellite, telling the transmitter that it has received a transmission. At this point, the transmitting satellite stops rotating and holds its attitude. If the satellites were using the actual onboard transmitters, the receiving satellite then begins estimating the range and bearing to the transmitting satellite, as well as the range rates. Using the simulated transmitter the satellite can simply difference the global states to determine the relative states. It uses this data to point its own transmitter towards the transmitting satellite, so that the two can achieve a front-to-front lock, with both satellites pointing their transmitters at each other. The satellite also simultaneously drives the relative velocity between the satellites to zero, nulling the range rates. Equation 2.3 shows the quaternion for the

rotation between the current attitude and the desired final attitude, where i_x, i_y, and i_z are the unit vectors in the satellite's body frame in the direction of the target. Equation 2.4 shows that the final quaternion (q_2) is the quaternion multiplication ($\otimes$) between the current attitude (q_1), and the normalized rotation quaternion (q_{12}).

$$q_{12} = \begin{pmatrix} 0 \\ \frac{i_z}{\sqrt{i_y^2+i_z^2}} \cos(0.5 \arccos(i_x)) \\ \frac{-i_y}{\sqrt{i_y^2+i_z^2}} \cos(0.5 \arccos(i_x)) \\ \sin(0.5 \arccos(i_x)) \end{pmatrix} \tag{2.3}$$

$$q_2 = q_1 \otimes \frac{q_{12}}{\parallel q_{12} \parallel} \tag{2.4}$$

This method uses only relative measurements for determining how to point. The satellites do use the global attitude data to perform the maneuver, but it would be possible to use only the onboard gyroscopes as well. Since there is only one transmitter, the satellite is not constrained about its body X axis. If constraint about the body X axis is desired, then more information, such as the satellites global attitude, is necessary. This information could come from a device such as a star tracker, or in the case of the SPHERES satellites, from the global attitude measurements.

2.2.5 Partnering

Each satellite performs the pealing maneuver until either it locates another satellite's transmitter, or another satellite locates its transmitter. The satellites that locate each other first become partners. So, if satellite 1 sees satellite 2's beacon, they become partners. This leaves the third satellite, which will parter with the first satellite that it locates (or locates it). So, there will be one satellite that will have two other satellites partnered with it, one satellite with one other satellite partnered with it, and one satellite with no other satellites partnered with it. Table 2.1 shows three possible partnering configurations (not a fully inclusive list). The satellite that has two other satellites partnered with it is given the Primary role. The satellite with

one other satellite partnered with it is given the Secondary role. Finally, the satellite with no other satellites partnered with it is given the Tertiary role.

Table 2.1: Three possible partnering configurations. Note: Not a fully inclusive list

Role	Satellite	Partner	Description
Primary	Sat 1	2	Sats 1 and 2 point at each other, Sat 3 points at 1
Secondary	Sat 2	1	
Tertiary	Sat 3	1	
Primary	Sat 2	3	Sats 2 and 3 point at each other, Sat 1 points at 2
Secondary	Sat 3	2	
Tertiary	Sat 1	2	
Primary	Sat 3	1	Sats 1 and 3 point at each other, Sat 2 points at 3
Secondary	Sat 1	3	
Tertiary	Sat 2	3	

2.2.6 Switch Target

The satellites are now in a configuration similar to the one in Figure 2-4. In the figure, the arrows indicate the direction of the satellite's transmitter. The numbers on the satellites indicate the role (1-Primary, 2-Secondary, 3-Tertiray). The final desired configuration is with one satellite pointing its transmitter at one other satellite, with no satellites pointing at each other. The simplest way to achieve this formation is for the Secondary satellite to switch and point towards the Tertiary satellite. After switching, the satellites are in the desired pointing configuration, and need move relative to each other into the final equilateral triangle formation.

2.2.7 Relative Ranging

There are several ways that the satellites could move relative to each other to achieve the final formation. The following method provides a valid solution to the problem by having two satellites move relative to a third. In this maneuver, the global atti-

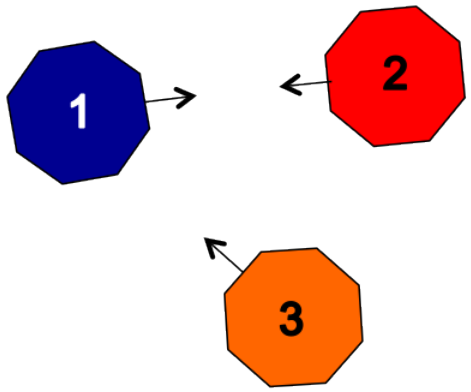

Figure 2-4: Possible intermediate configuration

tude data is also necessary on top of the relative range information. Each satellite communicates to the other satellites the direction that it is pointing its transmitter, in the global frame. The secondary satellite (S2) then controls its position to be the desired distance from the primary satellite (S1), in the direction that the primary satellite is pointing its transmitter ($\hat{d}_1$). This forms one side of the equilateral triangle. The other two sides are formed by the tertiary satellite (S3) using the direction all three satellites are pointing ($\hat{d}_1$, $\hat{d}_2$, and $\hat{d}_3$) to determine the unit vector from the primary satellite to the third corner of the equilateral triangle ($\hat{d}_{31d}$). The tertiary satellite moves the desired distance from the primary satellite in this direction. Figure 2-5 shows the secondary and tertiary satellites moving relative to the primary satellite to complete the formation, and Equations 2.5 through 2.7 show the calculations necessary to find $\hat{d}_{13d}$.

In this maneuver, two satellites move relative to a third. The satellites could decide together which satellite should remain stationary during the maneuver. This could be useful if one satellite is low on fuel, or if there are position requirements on the formation.

$$\alpha = \hat{d}_1 \cdot -\hat{d}_3 \tag{2.5}$$

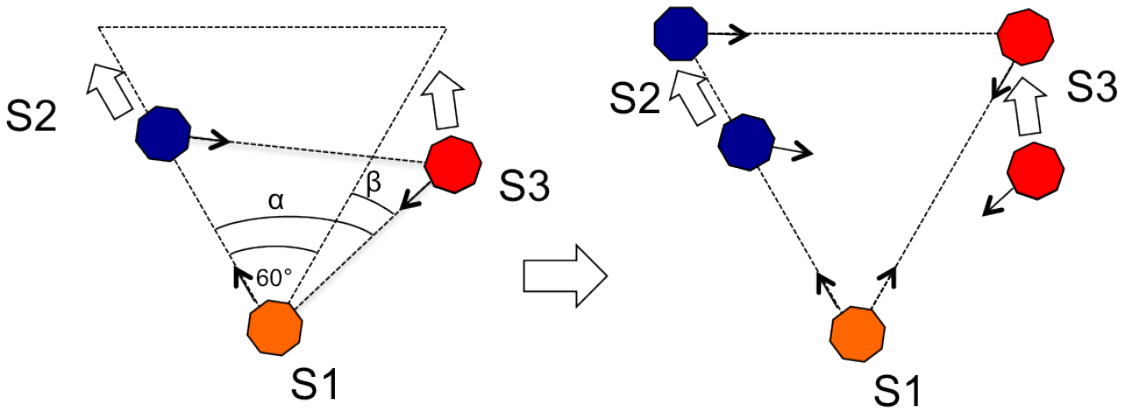

Figure 2-5: Secondary and Tertiary satellites move relative to Primary to complete the formation

$$\beta = \alpha - \frac{\pi}{3} \tag{2.6}$$

$$\hat{d}_{13d} = \frac{-\hat{d}_3 - \hat{d}_2 \sin\beta}{|-\hat{d}_3 - \hat{d}_2 \sin\beta|} \tag{2.7}$$

This method results in a set of cases in which the satellites will not be able to complete the ranging maneuver without colliding. When the satellites are near a linear configuration, as seen in Figure 2-6, the ranging maneuver may cause the Secondary and Tertiary satellites to collide. As a contingency, if the angle between $\hat{d}_1$ and $\hat{d}_2$ is less than 60°, the Tertiary satellite uses the direction defined by the cross product between $\hat{d}_1$ and $\hat{d}_2$ to maneuver out of this configuration. This assumes that the cross product is nonzero. If the cross product is zero, the Tertiary satellite could pick a direction perpendicular to $\hat{d}_1$ to avoid the linear case. Once the angle is no longer less than 60°, the Tertiary satellite continues with the ranging maneuver described above.

The satellites continue to point their transmitters towards their target satellite throughout the ranging maneuver. The test is then completed when the relative velocity between the satellites is sufficiently low and the distance between the satellites is within a tolerance of the desired positioning.

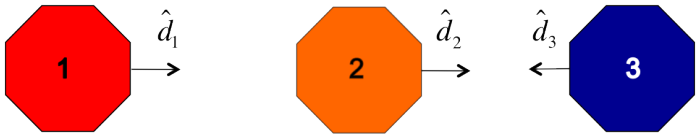

Figure 2-6: If the satellites are in this linear configuration, the Tertiary satellite (3) will be commanded towards the Secondary satellite (2). The figure shows the orientation after Secondary has switched to point towards Tertiary.

2.3 Chapter Summary

In this chapter an algorithm for the initialization of a three satellite formation using relative measurements was presented. The satellites first perform a three-dimensional search maneuver in order to locate the other satellites. Once another satellite is detected, the satellites use relative measurements to partner and point towards their desired target, as well as null any relative velocity. Once pointing is achieved, the satellites perform a ranging maneuver and create the desired final formation using both relative measurements and global attitude information. Results from testing this algorithm onboard the International Space Station in six degrees of freedom are presented in Chapter 4.

Chapter 3

Design of the Synthetic Imaging Maneuver Optimization Testbed

The previous chapter detailed how several satellites could assemble into a formation. After becoming a formation, the satellites could perform a coarse maneuver, such as a spiral, to begin coverage of the u-v plane. At certain points along the spiral, the satellites would make observations. These observations require precise control of the relative positioning between the satellites, as well as precise control of the path length of light entering the capture device. This chapter details how a staged control system could achieve the necessary precise control.

3.1 SIMO Overview

A staged control testbed has been developed through the Synthetic Imaging Maneuver Optimization (SIMO) program. The overall goal of the SIMO program is "to develop a methodology, calibrated through hardware-in-the-loop testing, to optimize spacecraft maneuvers to more efficiently synthesize images for missions such as Stellar Imager (SI)."[2] The testbed implements staged control techniques in order to act as an interferometry system. The testbed combines the coarse control of the SPHERES

satellites with a fast steering mirror to create fine pointing control and an optical delay line to perform fine phasing control. This chapter gives an overview of the project, including the requirements, and discusses the setup and the components in detail.

3.1.1 Requirements

The pointing requirements for the SIMO system were set by the requirements of the interferometer used for sensing the path length of the light. The interferometer allows a maximum offset of 1/4 of the beam diameter (6mm).[1] The maximum design separation (the maximum distance that the fine pointing stage will be from the interferometer) is set at two meters. This is based on the size of the testing area. Therefore, the fine stage must be able to control the position of the beam to 0.043°. The mechanical precision of the stage must be half of this, as the beam will deflect twice the angle of the mirror. So, the requirement for pointing control is 0.021°.

The phasing requirement is based on achieving a visibility function of at least 0.4. In order to meet this requirement, the system must be able to control the path length of the beam to at least $\lambda/4$.[25] The laser used has a wavelength of 632.99 nm, leading to a control requirement of 158.25 nm. Table 3.1 summarizes the requirements.

Table 3.1: SIMO requirements

	Control
Pointing	0.021°
Phasing	158.25 nm

3.1.2 Components and Beam Path

Figure 3-1 shows an overview of the system, with the following subsystems color-coded: pointing, phasing, and laser/optics. The system is designed to operate as a

Michelson interferometer. The pointing subsystem (blue) controls the positioning of the beam, and the phasing subsystem (green) controls the path length. The path that the laser beam follows can be seen in Figure 3-2.

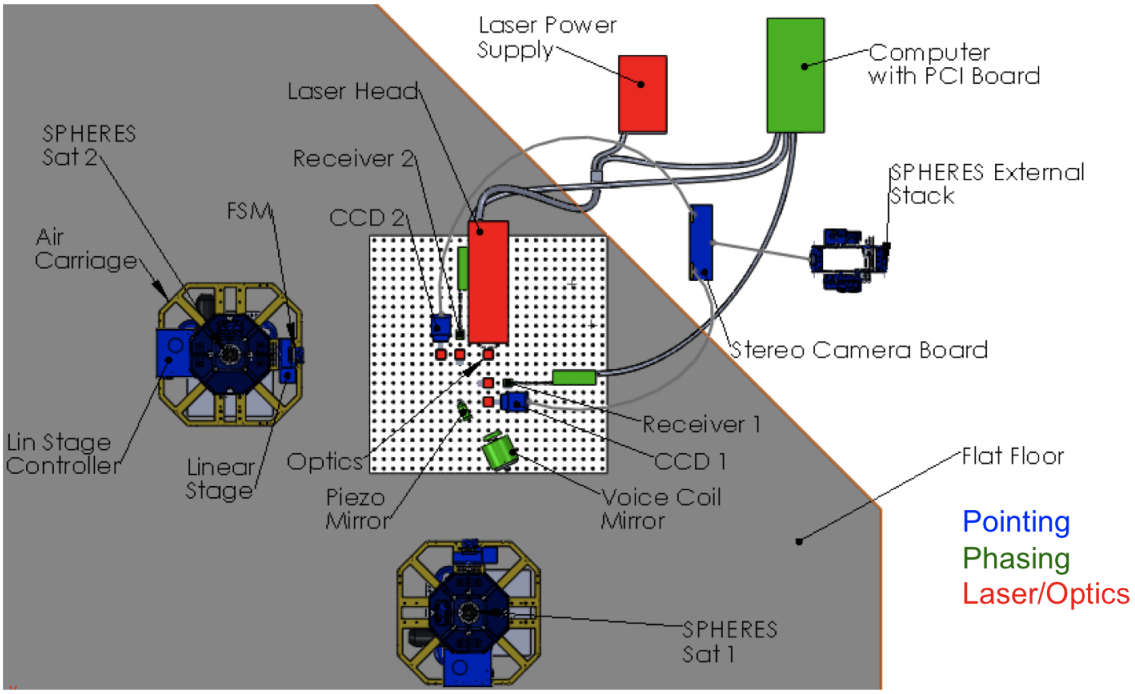

Figure 3-1: Overhead view of the final SIMO setup

The main components are as follows:

- Laser and Optics
  - Agilent 5517B Laser Head
  - 2 polarizing beam splitters
  - 3 50% power beam splitters
- Pointing
  - 2 SPHERES satellites
  - 1 Fast Steering Mirror (FSM) per satellite
  - 1 Newmark Microslide Linear Stage per satellite
  - 1 Blackfin SRV-1 camera per satellite
  - SPHERES external stack
- Phasing

- 1 Agilent 10780F Remote Receiver per satellite
- Brüel & Kjær Mini-shaker Type 4810
- Physik S325 Piezo Mirror
- Agilent N1231B PCI Board

Figure 3-2 shows the path that the laser beam follows after exiting the laser head. The beam exits the laser and immediately passes through a power beam splitter. The downward path (in the view of Figure 3-2) first passes through a polarizing beam splitter. The beam splits, and one path travels to the left (the green path), passing through a quarter wave plate (QWP), then reflects off a retro-reflector, passes through the QWP again, and then continues through the beam splitter to the receiver. The other beam (the blue path) exits the polarizing beam splitter, passes through a QWP, and then continues to another power beam splitter. The beam splits left and down, but the output of the beam that passes to the left is suppressed. The beam that exited downwards continues and reflects first off the voice coil mirror, then the piezo mirror, and travels to the fast steering mirror (FSM) attached to the satellite. The FSM reflects the beam back to the piezo mirror, then to the voice coil mirror, then to the power beam splitter. Half of the beam's power reflects to the right, into the camera, which is used for pointing. The other half continues to the polarizing beam splitter, where it first passes through the QWP, then reflects to the right into the receiver. The two beams that entered the receiver then are compared by the sensing system to determine the path length.

The path the exited the laser and turned to the left through the first power beam splitter follows a similar path to the downward beam, but does not pass through an optical delay line (the piezo and voice coil mirrors).

3.1.3 Concept of Operations

The proposed concept of operations for SIMO are as follows:

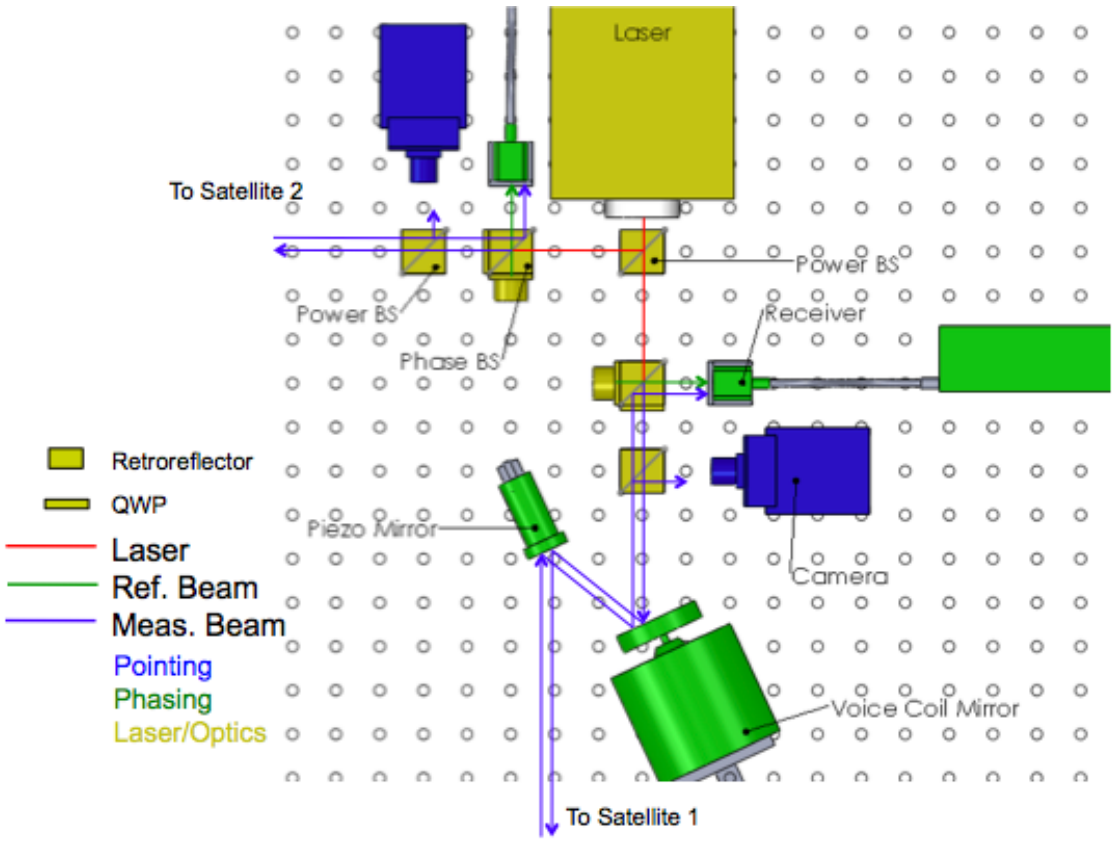

Figure 3-2: Overhead view of the path that the laser beam travels. Note: incoming and outgoing laser paths will be collinear; they are shown as parallel for ease of interpretation.

1. The two SPHERES satellites use the metrology system to travel to a predetermined location and hold coarse position and attitude.

2. Each linear stage compensates for error in its respective satellite's positioning using data from metrology, and the FSMs compensate for error in rotation.

3. The FSMs use pointing information from the CCDs to point accurately.

4. Once both receivers are sending data, the optical delay line uses information from the receivers to adjust the beam's path length and achieve phasing.

As of May, 2010, the testbed is not capable of completing the entire concept of operations, as the project is still underway. Currently the testbed is capable of having the FSM point accurately, using the data from the camera, while one satellite

is floating on the flat table. The phasing system is also able to measure path length, but only using fixed mirrors.

3.2 Laser and Optics

3.2.1 Laser

The laser used for the testbed is a Helium-Neon Agilent (HP) 5517B Laser Head. The laser beam is 6mm in diameter and is collimated and coherent. The coherence length is such that an optical range of 40 meters is possible (this setup uses a maximum of 4 meters of path length). The beam consists of two orthogonally polarized frequency components. Of the two components, f_1 is horizontally polarized and f_2 is vertically polarized, and f_2 is at a higher frequency. Before the beam leaves the laser head, part of it is sampled to find the difference in frequency between the two polarizations. This frequency difference is known as the Reference Frequency, is in the range of 1.9-2.4 MHz, and is a TTL square wave. The Reference Frequency is used in determining the path length, which is discussed in Section 3.4.4. A summary of the characteristics of the laser can be seen in Table 3.2.[1]

Table 3.2: Agilent 5517B Laser Head specifications[1]

Mass	3.4 kg
Power	+15 V ±0.3 V at max 2.2 A −15 V ±0.3 V at max 0.02 A
Beam Type	He-Ne, Continuous, Two-Frequency
Maximum Beam Power	1 mW
Minimum Beam Power	120 μW
Beam Diameter	6 mm
Wavelength	632.99137 nm ±0.02 ppm
Class	Class II
Reference Frequency	1.9-2.4 MHz

3.2.2 Beam Splitters

A total of three 2 cm 50% power beam splitters and two 1 cm polarizing beam splitters are used in the setup. The 50% power splitters pass half of the beam's intensity straight through and redirect the other half 90°. The polarizing beam splitters split the beam by polarization, passing one polarization straight through and redirecting the other polarization 90°. Also attached to the polarization splitters are quarter wave plates (QWP), which change the phase of the beam by one fourth of the wavelength of the light. When the beam returns to the polarizing splitter, it passes through the QWP again, and the phase of the beam has shifted by one half of the wavelength. This half-wavelength shift corresponds to a change in polarization. So, the beam that previously passed through the polarizing splitter has shifted polarization and will now redirect 90°, and the beam that was previously redirected will now pass straight through. The polarizing beam splitters are used because the receivers used in the sensing system (discussed in Section 3.4.4) require the two incoming beams to have opposing polarizations.

3.3 Hardware Design: Pointing

The pointing system consists of coarse control, fine control, and sensing. The coarse control is provided by the SPHERES satellite, the fine control is provided by a linear stage and a fast steering mirror, and the sensing is provided by the SPHERES metrology and a CCD.

A block diagram of all of the connections between the components can be seen in Figure 3-3. Starting at the CCD, the path is as follows.

1. The CCD images the laser beam and calculates the centroid location. The CCD then sends the centroid to the SPHERES external stack through a UART connection.

2. The stack communicates the centroid to the SPHERES satellite, which is holding its position based on data from the metrology system, through the SPHERES communication channel. The satellite determines how to move the linear stage and FSM using data from the SPHERES metrology and the current camera centroid.

3. The satellite transmits this information through an RS-232 convertor and then to a PIC 18F8722 Microcontroller through a UART connection. The PIC then:

   (a) outputs the desired FSM input through its SPI port to a MAX5523 Digital to Analog Convertor. The DAC then converts the digital signal to analog and sends it to two LM4861M amplifiers, which are connected to the FSM.

   (b) sends the linear stage position through its second UART connection to a TTL to RS-232 convertor, then to the linear stage controller, which transmits the data to the linear stage.

This process is performed by both satellites. A diagram of the connections between the satellite, linear stage, and FSM can be seen in Figure 3-14

3.3.1 Coarse Position and Rotation: SPHERES (Actuation and Sensing)

The coarse pointing control is provided by the SPHERES satellite. The satellite uses a PID controller to hold its position at a pre-defined location that allows the laser beam to hit the FSM. The satellite uses the SPHERES metrology system, as well as internal measurements, to estimate its position, velocity, attitude, and rotation rate. Figure 3-4a shows the precision of the measurements system for position is approximately ± 1.5 mm. Figure 3-4b shows the precision of the SPHERES measurement system for rotation about the satellite's body Z axis. The precision is approximately ± 0.5 degrees.

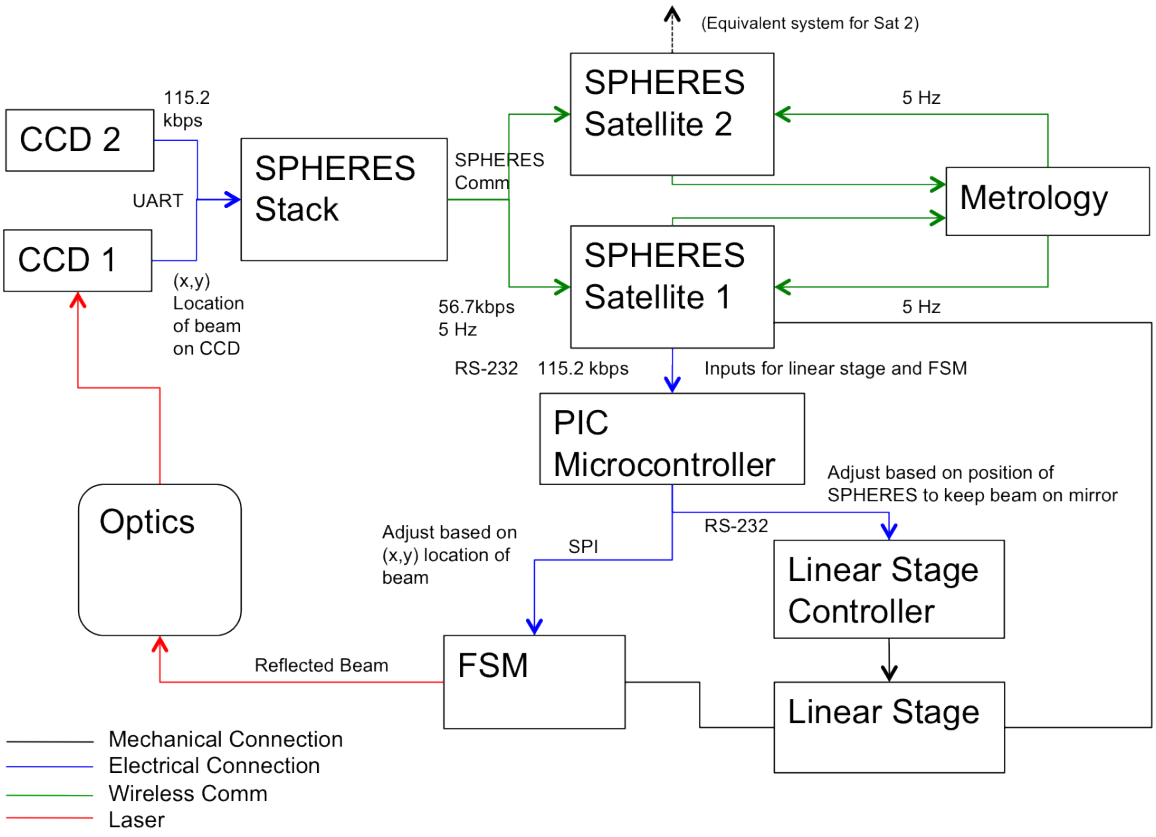

Figure 3-3: Components of the pointing system and the connections between them

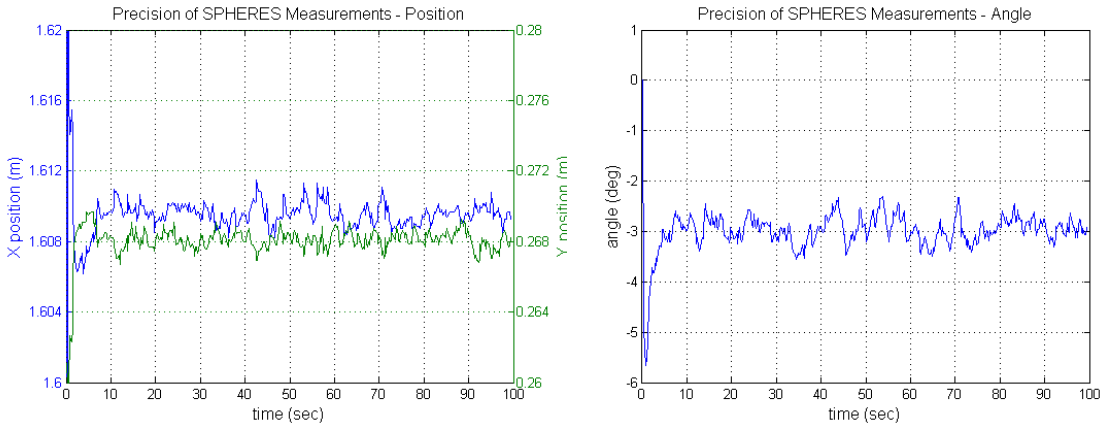

(a) Position (b) Rotation

Figure 3-4: Precision of the SPHERES measurement system

The SPHERES satellite will be required to actively hold its position and rotation throughout the test. It is important that the resolution of the satellite's control is within the range of the linear stage and fast steering mirror to facilitate staged control. The satellite uses separate PID controllers for attitude and position control. The inputs to the attitude controller are the error in the attitude, measured in quaternions, and the error in the rotation rates. The inputs to the position controller are the error in position and velocity. The outputs of both controllers are torques. These torques are summed together and are used as the inputs in the mixer function. The mixer determines, based on the desired torques and the satellite's current state, what thrusters to fire, and for how long. The gains used for the controllers have been tuned throughout the development of the SPHERES testbed, and have been used in several previous tests.

The results from a closed loop test using the PID attitude and position controllers are below. Figure 3-5a shows error in position while the satellite attempts to hold position. The plot shows that the satellite is capable of approximately centimeter-level control in position. Figure 3-5b shows the error in Z rotation during the position hold maneuver. The plot shows that the satellite is capable of sub-degree control in rotation. The satellite is performing both attitude and position control at 2 Hz during the test. The PID gains used in the controller were not designed specifically for precisely holding position. It may be possible to modify the gains to improve the precision of the satellite's actuation. From Figure 3-5a it appears that the system is slightly underdamped. Modifying the gains to reach critical damping could improve the precision of the satellite's control.

3.3.2 Camera (Sensing)

A Surveyor SRV-1 Blackfin Camera, as seen in Figure 3-6, is used to aid in fine pointing. The camera uses an OmniVision OV9655 charged coupled device (CCD)

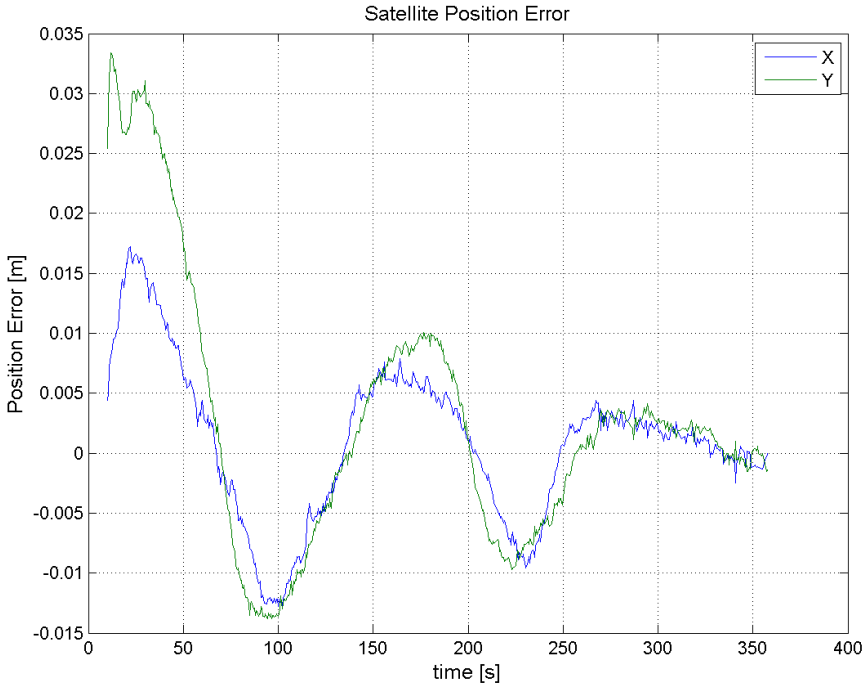

(a) Position

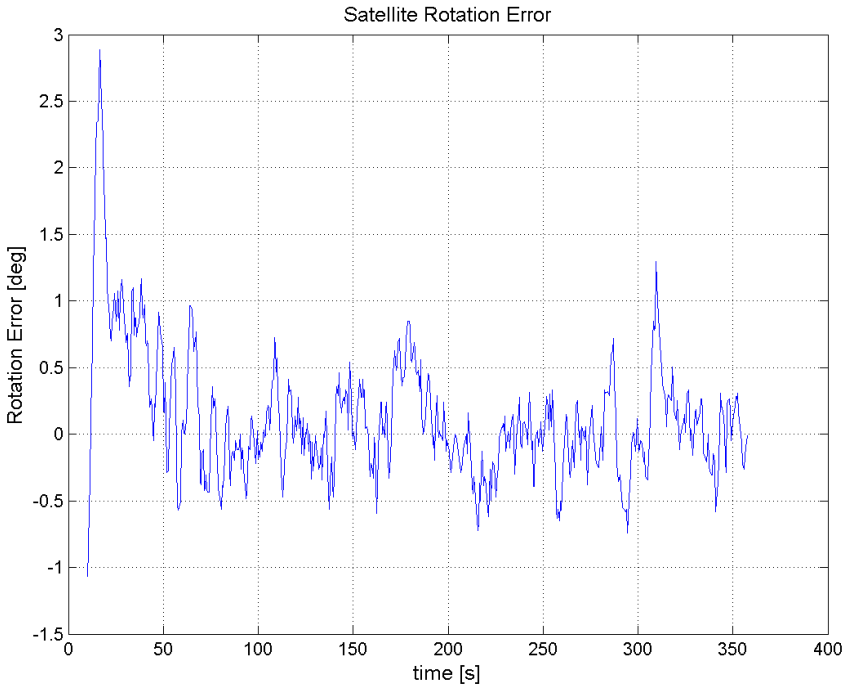

(b) Rotation

Figure 3-5: Closed loop error in the satellite's position and rotation

for imaging. Table 3.3 gives an overview of the specifications of the camera. After reflecting off the FSM, the laser beam returns through the beam splitter and is imaged by the CCD. The beam lands on a screen attached to the beam splitter. This allows the camera to track the beam over the full range of the beam splitter.

Table 3.3: SRV-1 Blackfin Camera with OV9655 CCD specifications [24][30]

I/O	UART
Power	3.3 VDC
Max Resolution	1280x1024
Min px Size	3.18 μm x 3.18 μm
Field of View	90°
Lens	3.6mm f2.0
Processor	500MHz Analog Devices BF537

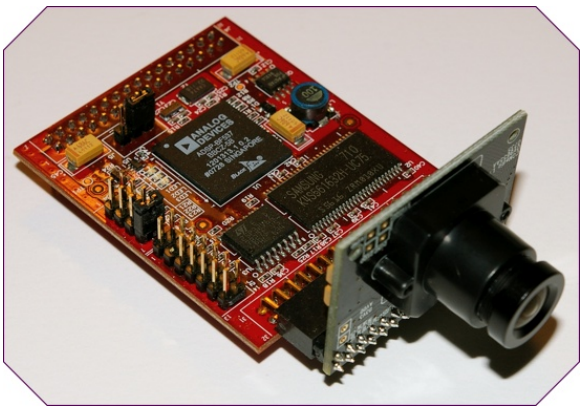

Figure 3-6: Surveyor SRV-1 Blackfin Camera

The camera runs an onboard centroiding algorithm and outputs the result of the calculation through its UART port. The data is sent to the SPHERES stack through the expansion port, and that data is then sent to the controlling satellite using the SPHERES communication channel.

There are several methods that can be used for calculating the centroid. The following algorithm is both accurate and efficient. Equation 3.1 is used to calculated the centroid for each axis, where I is the intensity of pixel (x, y), with a total of (n_x, n_y)

pixels in the CCD. The algorithm scans through the pixels, and if the intensity is over a specified threshold, then the moment of that pixel (the intensity times the pixel number) is added to the centroid. The sum over all the moments is then divided by the number of pixels. The camera calculates the centroid for both the horizontal (X) and vertical (Y) axes. More discussion of centroiding algorithms can be seen in [12].

$$Centroid_X = \frac{\sum_{x=1}^{n_x} x \cdot I_x}{\sum_{x=1}^{n_x} I_x} \text{ and } Centroid_Y = \frac{\sum_{y=1}^{n_y} y \cdot I_y}{\sum_{y=1}^{n_y} I_y} \tag{3.1}$$

In order to reduce the time that the algorithm takes to find the centroid, the number of pixels that the algorithm scans is reduced. The algorithm searches the full range in the X (horizontal) direction, but only uses the middle half of the Y (vertical) direction. So, the CCD is effectively 680 x 270 pixels. Since the satellite is constrained to a plane, the FSM will be able to point the vertical axis close to the middle of the camera. The vertical centroid is still necessary, as there are mounting imperfections, as well as imperfections in the FSM, that lead to the vertical portion of the beam not pointing perfectly towards the centroid. Closed-loop control eliminates these inaccuracies.

The contrast of the CCD is reduced so that high-intensity pixels that are not from the laser are eliminated, achieving a more accurate centroid. Figure 3-7 shows what the CCD is centroiding during a test. The red box indicates the screen that is placed in front of the beam splitter before the camera. The vertical green line indicates the position of the calculated horizontal centroid (there is no line for the vertical centroid, but it is calculated), and the large dot is the laser.

The position of the screen in relation to the beam splitter and the camera can affect the range and resolution of what the camera can sense. It is desired for the camera to be able to see the entire range of possible motion of the laser beam. Figure 3-8 shows a possible placement for the screen and camera. In the figure, d_s is the distance from the edge of the beam splitter to the screen, d_c is the distance from the

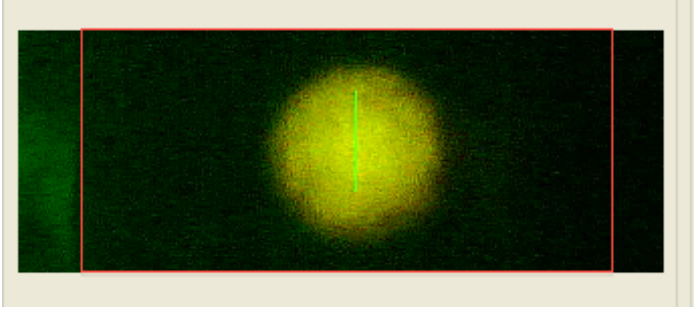

Figure 3-7: View of what the CCD sees during centroiding. The red box indicates the screen that is placed in front of the beam splitter.

screen to the camera, and l_s is the length of the screen. The screen should be long enough so that it can see the beam when the beam is going through either edge of the beam splitter (as shown in the figure). The camera has a field of view (θ_{FOV}) of 90°, so the minimum distance that the camera should be from the screen is $a/\sqrt{2}$.

Since the laser beam is collimated, the beam will be 6 mm on the screen regardless of d_s. Increasing d_c will decrease the number of pixels that the beam takes up. The width of the beam in pixels will therefore be $1920/d_c$ (with d_c in mm). When d_s is larger, a small change in angle will result in more of a change in pixels. Therefore, the sensitivity of the camera increases with a larger d_s. However, if d_s is too large, then the beam won't take up as many pixels, resulting in a less accurate calculation. These tradeoffs drive the positioning of the camera and the screen.

Placing the screen immediately next to the beam splitter ($d_s = 0$) was decided to be used for the setup. The sensitivity is still high at this position, as is the accuracy. Figure 3-9 below shows the results of a static test in which the camera measured the position of the laser beam. When the centroid is communicated from the camera to the satellite, the resolution of the centroid calculation is 0.1 px, so that is the maximum precision that the camera can provide. It would be possible to communicate at a higher precision, but 0.1 px was determined to be an adequate precision. The plot shows that the camera is capable of precision on the order of ±0.4

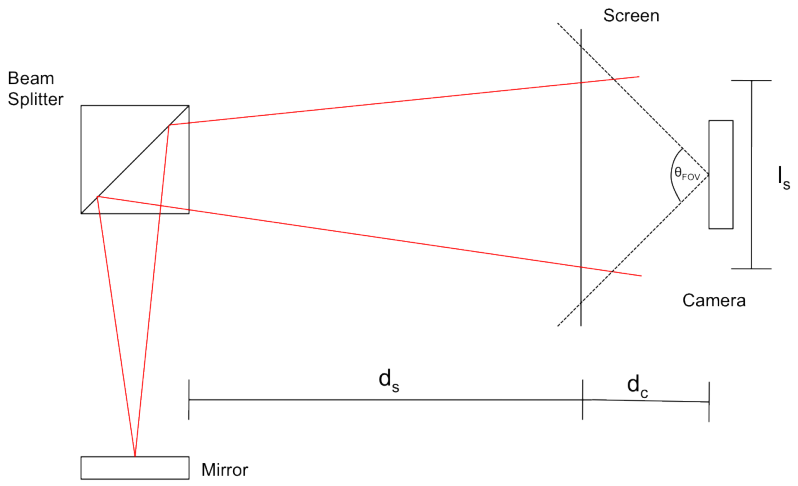

Figure 3-8: Placement of the screen and camera affects the range and resolution of the camera

px. There was a small amount of drift of the beam during the measurement, due to the FSM. The rest of the error represents the system noise.

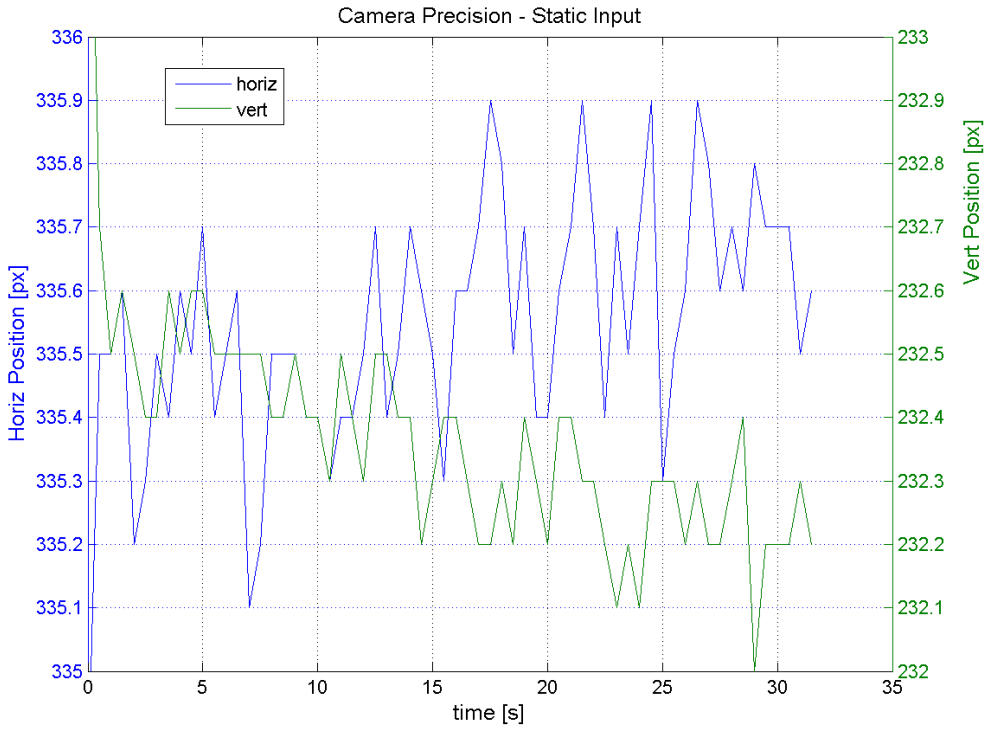

Figure 3-9: Camera measurements with static input

3.3.3 Fine Positioning: Linear Stage (Actuation)

Since the diameter of the FSM is less than the precision that the SPHERES satellite can control, it is necessary to add an intermediate stage to ensure that the laser beam will always be able to hit the FSM. A Newmark Microslide was chosen to perform this task. The stage is capable of moving ± 1.27 cm, with a repeatability of 5 μm and a maximum travel speed of 1.016 cm/s. The stage weighs 0.454 kg and has easy access holes to mount the stage to the satellite, as well as the FSM to the stage. [23] The linear stage's characteristics are summarized in Table 3.4.

Table 3.4: Newmark Microslide linear stage properties

Range	2.54 cm
Resolution	0.02 μm
Max Velocity	1.016 cm/s
Mass	0.454 kg
Repeatability	5 μm

The linear stage is mounted to the satellite via an adapter plate, as seen in Figure 3-10. The stage moves parallel to the satellite face it is mounted to, in the horizontal direction. The FSM is then mounted to the linear stage, using a custom made mount.

The stage is driven by a MicroLYNX-4 single axis stepper motor controller, as seen in Figure 3-11. The controller is powered by a 24V, 1.5A DC input. The input to the controller is RS-232, and there are two outputs: one provides power to the linear stage's motor, and the other provides the signal to control the movement. As the SIMO testbed progresses it may be desirable to use a smaller controller that can be attached to the satellite. The initial testbed will attach this controller to the satellite's air carriage.

The satellite controls the movement of the linear stage. The satellite sends commands to the PIC processor through the expansion port, which then converts the

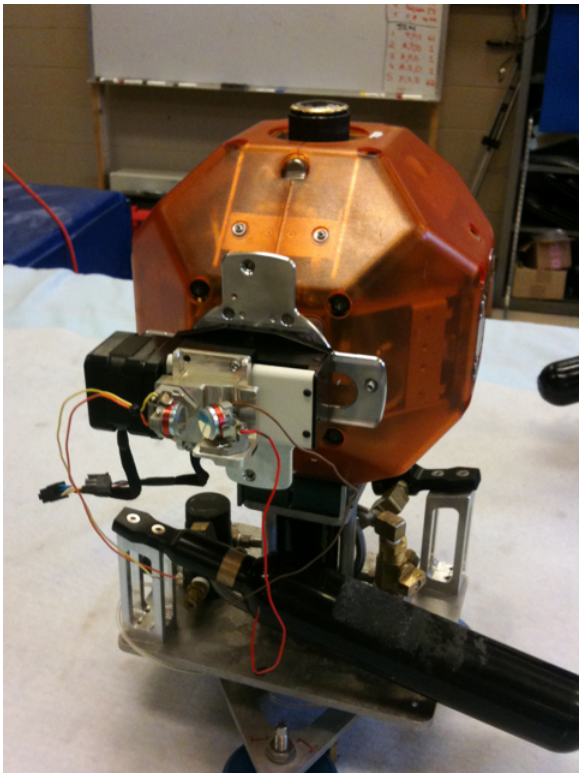

Figure 3-10: Linear stage and FSM attached to the satellite via an adapter plate

commands into the proper input for the linear stage controller. The commands are then sent to the controller (after passing through a TTL to RS-232 converter) through the PIC processor's second UART port. The controller accepts the input and then commands the linear stage.

The linear stage is controlled based on the error in the satellite's position and attitude. The controller is configured to accept inputs in increments of 0.1 mm. Equation 3.2 shows the calculation of the desired position of the linear stage,

$$uls_k = \frac{Y_k}{\cos Z_k} + d_{mirror} * \tan Z_k \tag{3.2}$$

where Y_k is the satellite's error in the frame's Y axis, d_{mirror} is the distance from the center of the satellite to the desired position of the mirror, and Z_k is the error in the satellite's Z rotation, calculated in Equation 3.4.

Figure 3-11: MicroLYNX stepper motor controller for Newmark Microslide

3.3.4 Fine Rotation: FSM (Actuation)

The fast steering mirror (FSM) corrects for errors in the satellite's rotation. The mirror can be seen in Figure 3-12. The FSM has two mirrors, actuated by voice coils, that independently control the vertical and horizontal return of the beam. The mirror controlling the horizontal axis is rotated 45 degrees to the incoming beam, and is the mirror on the right in Figure 3-12. The vertical axis mirror is mounted 90 degrees to the incoming beam. The mirrors are set up such that when aligned properly, the return beam will be collinear to the incoming beam. Both mirrors are controlled by a differential voltage. The mirrors were previously used in the Precision Pointing Optical Payload, where the dynamics of the mirrors were experimentally determined. A summary of the specifications can be seen in Table 3.5.[12]

The FSM uses two different measurements to determine how to point. If the camera (see Section 3.3.2) can see the laser beam, then the FSM uses the error between a reference centroid and the current centroid to determine how to point. If the error is too large, and the beam is not hitting the camera, then the FSM uses the error in the SPHERES rotation measurements from the desired position to determine

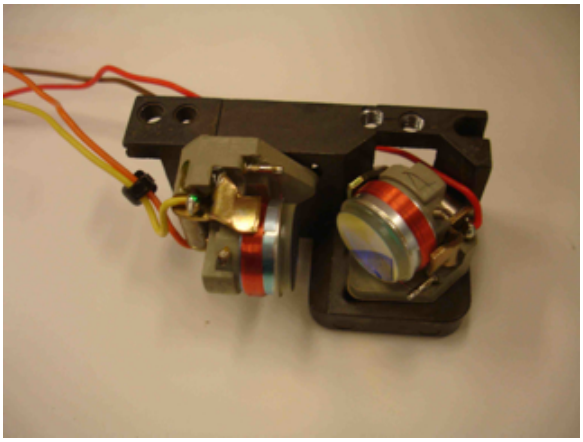

Figure 3-12: Two axis fast steering mirror

Table 3.5: Fast Steering Mirror properties

Mirror Range	$\sim\pm 12^{\circ}$
Ave. Resistance	$\sim 7.7\ \Omega$
Damping Coeff.	~ 0.3
Natural Frequency	~ 68.97 Hz (433.32 rad/s)

how to point.

The FSM is mechanically connected to the satellite via the linear stage (see Section 3.3.3). The FSM is powered and controlled through the SPHERES expansion port. Data is sent through an RS-232 connection to a PIC 18F8722 microcontroller. The PIC receives the UART data (after conversion to TTL levels) and then converts it into the necessary form for the MAX 5523 Digital to Analog Converter (DAC) and outputs the data through the SPI port. The DAC then connects to two LM 4861 amplifiers. Figure 3-13 shows the amplifier circuit diagram. A diagram of the connections can be seen in Figure 3-14.

A resolution of approximately 0.01° is desired for the FSM, in order to exceed the requirements. The DAC has an internal reference voltage of 3.885V. Using Equation 3.3, and choosing R_f and R_i, the range of the mirror can be set. The resolution is

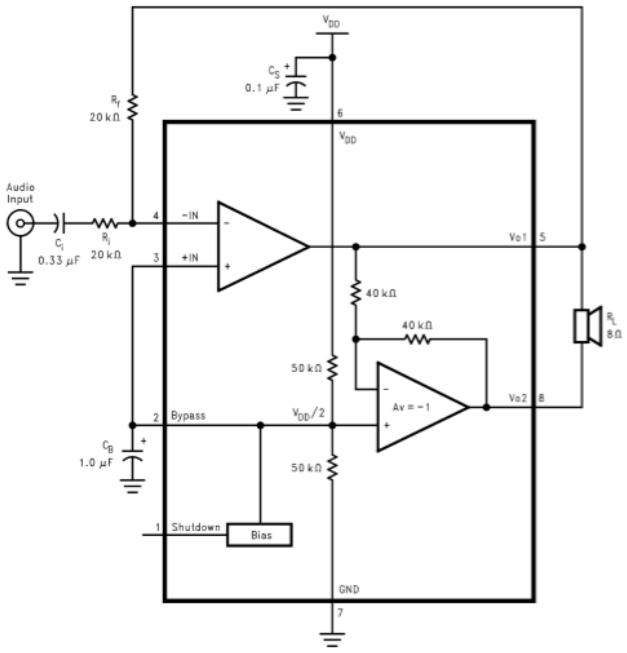

Figure 3-13: LM4861 amplifier circuit [22]

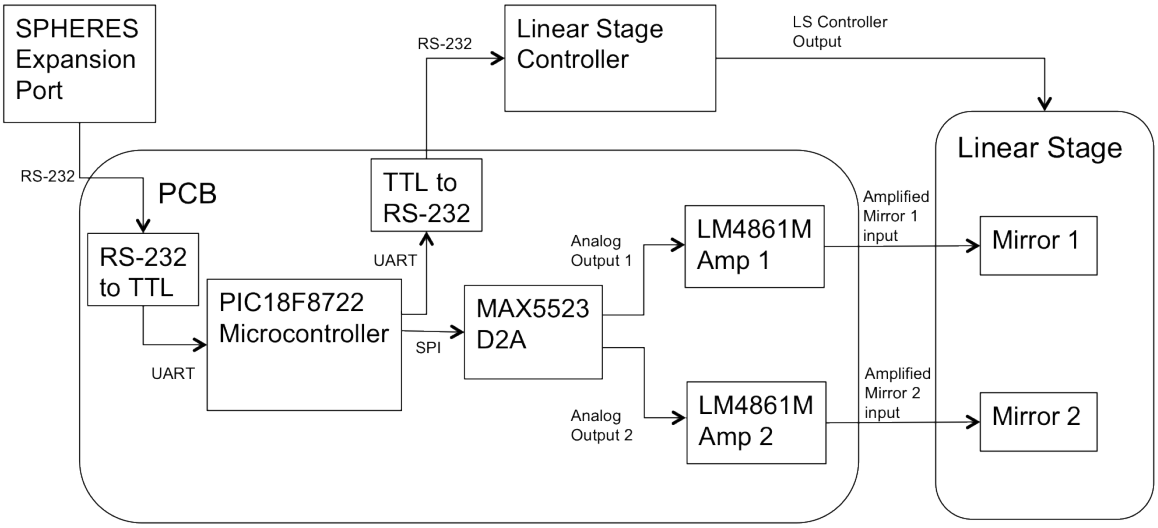

Figure 3-14: Diagram of the connections between the satellite and the linear stage and FSM

then set by the precision of the DAC.

$$V_{out} = \frac{R_f}{R_i}(2V_{in} - V_{ref}) \tag{3.3}$$

In the equation, Vin is variable and the other parameters are set. Choosing $R_f = 100k\Omega$ and $R_i = 47k\Omega$ gives a range of ± 1.828V, or $\pm 5.32°$. The DAC has 10 bit precision, which means that the resolution of each mirror is 0.00357 V or 0.0104° for each count of the DAC. A summary of the specifications of the FSM can be seen in Table 3.6

Table 3.6: Specifications of the FSM with MAX5523

Range	$\pm 5.32°$
Resolution	0.0104°

When the camera can see the laser beam, the FSM can use precise closed loop control to point accurately. When there is no camera data, the FSM must actuate based only on the satellite's attitude error about its Z axis. The Z error is calculated in Equation 3.4,

$$Z_k = \arctan \frac{2(Q_{3e}Q_{4e} + Q_{1e}Q_{2e})}{1 - 2(Q_{2e}^2 + Q_{3e}^2)} \tag{3.4}$$

where Q_{1e} through Q_{4e} are elements one through four, respectively, of the error quaternion.

The satellite incorporates the Z error into the following control law,

$$u_k = K_p Z_k \tag{3.5}$$

where Z_k is the error in the satellite's Z rotation, K_p is the proportional gain, and u_k is the control at time k.

When the camera can see the laser beam the FSM can use the measurements to

add integral control in the form of the following equation:

$$u_k = u_{k-1} + K_I E_k \tag{3.6}$$

where u_{k-1} is the control during the previous control period, K_I is the integral gain, and E_k is the error in the centroid from the reference centroid.

3.4 Hardware Design: Phasing

The objective of the phasing system is to use the optical delay line to adjust the length of one of the laser beam paths in order to achieve phasing between the two paths. The phasing system consists of the SPHERES satellite, a voice coil actuated mirror, a piezo actuated mirror, and an interferometry measurement system. Figure 3-15 shows a block diagram of the components of the phasing system.

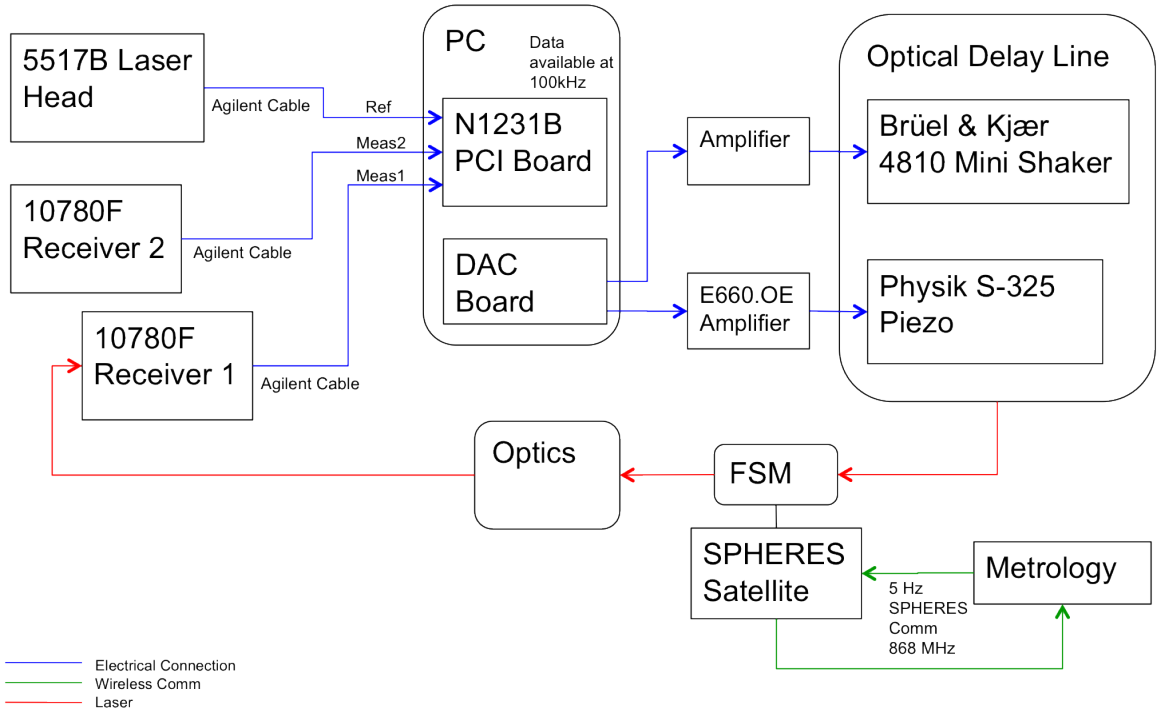

Figure 3-15: Components of the phasing system

Once the satellites are in position and the FSM has achieved accurate pointing, the optical delay line can perform phasing. After reflecting off the FSM and passing through the optics, the laser beam hits the two receivers, which send an interference signal to the PCI board. The board then calculates path length differences in the two paths. The two path lengths are then sent to MATLAB, which performs calculations on the path lengths to determine how to adjust the optical delay line to achieve the desired path length. MATLAB communicates with a digital to analog converter, which then outputs the signals to the optical delay line, through amplifiers.

3.4.1 Coarse Phasing: SPHERES (Actuation and Sensing)

The SPHERES satellites are a part of the control system in that they will be required to hold position while the other components are completing the phasing portion. The satellite is accurate in measuring its position and attitude to approximately ± 1.5 mm and $\pm 0.5°$and is capable of controlling its position and attitude to centimeter and sub-degree precision, as discussed in Section 3.3.1.

3.4.2 Medium Phasing: Voice Coil Mirror (Actuation)

A Brüel & Kjær Mini-shaker Type 4810 is used as one side of the optical delay line. The Mini-shaker, seen in Figure 3-16 is voice coil actuated. Specifications can be seen in Table 3.7. The input is a DC voltage, from -1.8A to +1.8A, which displaces the attached flat mirror ± 3 mm. The signal will be sent to the shaker through an amplifier (which has not been chosen as of May, 2010) by the digital to analog converter (which also has not been chosen as of May, 2010) inside the PC. The resolution of the Mini-shaker's movement will be driven either by the resolution of the DAC or by the noise in the system (whichever is larger).

Figure 3-16: Brüel & Kjær Mini-shaker Type 4810

Table 3.7: Brüel & Kjær Mini-shaker Type 4810 specifications[3]

Frequency Range	DC to 18kHz
Maximum Displacement	6 mm (peak to peak)
Coil Impedance	3.5 Ω at 500 Hz
Max Input Current	1.8 A
Mass	1.1 kg

3.4.3 Fine Phasing: Piezo Mirror (Actuation)

The fine stage used for phasing is a Physik Instrumente S-325 piezoelectric fast steering mirror, as seen in Figure 3-17. The stage is controlled by three piezoelectric linear actuators. When all three actuators are actuated together, the mirror attached on the end moves in the desired linear motion along the long axis of the piezo. The piezo has a range of 30 μm and a resolution of 0.5 nm. A summary of the specifications can be seen in Table 3.8.

Figure 3-17: Physik Instrumente S-325 piezo FSM

Table 3.8: Physik Instrumente S-325 specifications[26]

No. of Axes	3
Open-Loop Travel	30 μm
Input Range	0-100 V
Open-Loop Resolution	0.5 nm
Mass	0.065 kg
Connector	LEMO

The piezo is driven by three Physik Instrumente E-660.OE amplifiers, one for each piezo axis. The amplifiers are on a single board and are powered by a 12 V DC power supply. An input voltage of $\pm$ 1 V is converted to a 0-100 V output. The input comes from the digital to analog converter board inside the PC, similar to the Mini-shaker. The outputs of the amplifier are connected to the three axes of the piezo. Since it is desirable to move the mirror only in the piston mode, all three amplifiers are given the same input. The amplifier board can be seen in Figure 3-18.

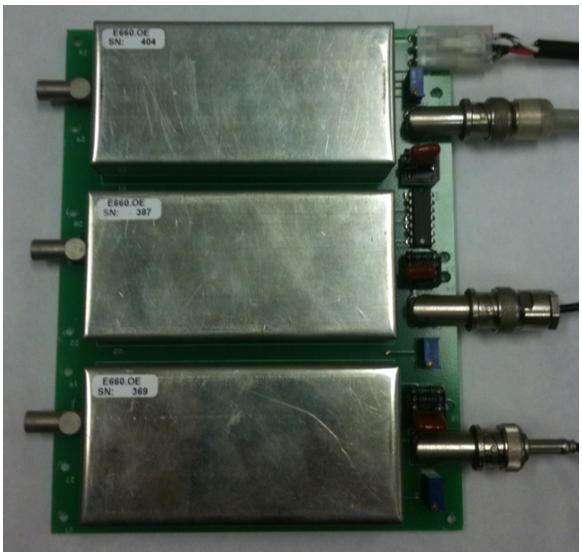

Figure 3-18: Physik Instrumente E-660.OE amplifiers

3.4.4 HP Receiver/Board (Sensing)

The sensing for the phasing system is performed by an Agilent interferometry system. Two Agilent 10780F Remote Receivers, along with an Agilent N1231B PCI Board are used to calculate path length differences in the two paths. Both can be seen in Figure 3-19.

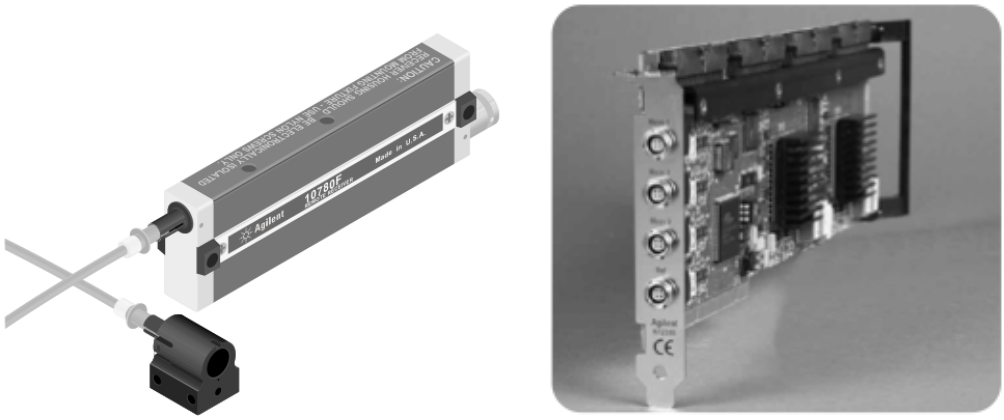

(a) Agilent 10780F Remote Receiver (b) Agilent N1231B PCI Board

Figure 3-19: Agilent receiver and PCI board

The 10780F Remote Receiver consists of a lens and polarizer that are connected to the receiver body by a fiber optic cable. The lens passes light through a polarizer, which is oriented at 45°to the horizontal and vertical axes of the housing, and then the interference signal between the two polarizations is sent through the fiber optic cable to the receiver body. The light is then imparted on a silicon PIN photodiode. After transforming the signal, the receiver body outputs a differential square wave at the Doppler-shifted split frequency. An LED on the receiver body indicates when sufficient light is passing through the system (but does not necessarily indicate proper alignment).

The frequency of the differential square wave that is sent by the receiver is then called the Measurement Frequency. The signal is sent to the N1231B PCI board, which also receives a similar signal from the Laser Head (see Section 3.2.1), called

the Reference Frequency. The difference between the Measurement Frequency and the Reference Frequency is used to calculate the path length. At initial measurement the path length will be zero, and will be non zero if any of the optics (i.e., the FSM on the satellite) move. This is now the signal used for phasing.

Both 10780F receivers will send a signal that can be used to calculate path length difference. The objective is to have the two path lengths move together, within a tolerance defined by the requirements (see Table 3.1). The ODL adjusts the length of one of the paths to achieve this.

The PCI board is housed and powered by a PC. The PC runs a program that retrieves the data from the PCI board when available. MATLAB then communicates with the program to access the data and output it to DAC board, which connects to the ODL. The system is capable of a resolution of 0.15 nm ($\lambda/4096$), meeting and exceeding the sensing requirements.

3.5 Stage Overlap

If there were a single actuator that had large stroke, high bandwidth, and high resolution, staged control would not be necessary. However, actuators that have a large stroke tend to have lower bandwidth and resolution, and actuators with high bandwidth and resolution tend to have a smaller stroke. In order for staged control to function properly, it is desirable for the stages to have overlapping strokes and bandwidths.

Table 3.9 summarizes the range, resolution, and bandwidth of the pointing actuators. There is overlap between the strokes of the stages, as well as the bandwidths. A plot of the overlap can be seen in Figure 3-20. As seen in the figure, the overlap between the linear stage and the satellite is small. This is not currently a concern, as the linear stage is capable of moving much faster than the satellite while the satellite

is attempting to hold position. Even if the stage is near saturation, the laser beam should be able to remain on the FSM. Efforts will also be made to improve the precision of the satellite's actuation abilities by modifying the PID control gains, which would improve the overlap.

Table 3.9: Range, resolution, and bandwidth of the pointing stages

	Range	Resolution	Bandwidth
SPHERES Sat. Position	2 m	1 cm	0.2 Hz
SPHERES Sat. Rotation	$\pm 180^\circ$	1°	0.2 Hz
Linear Stage	± 1.27 cm	0.5 μm	1.02 cm/s[1]
FSM	$\pm 5.32^\circ$	0.0104°	60 Hz[2]

Table 3.10 summarizes the range, resolution, and bandwidth of the phasing actuators. There is not sufficient overlap between the SPHERES satellite and the voice coil mirror, but there is overlap between the voice coil and piezo mirrors. A plot of the overlap can be seen in Figure 3-20. There is also adequate bandwidth overlap. The SPHERES satellite is not accurate enough to ensure that there will be overlap at all times between the satellite and the voice coil mirror. This will result in saturation of the voice coil. Improvement in the overlap between the satellite and the voice coil may be possible by improving the SPHERES PID controller. This should be possible, as the controller is not designed specifically for precisely holding position. If this is not possible, methods to desaturate the voice coil will need to be employed to succeed in achieving phasing.

Table 3.10: Range, resolution, and bandwidth of the phasing stages

	Range	Resolution	Bandwidth
SPHERES Sat. Position	2 m	1 cm	0.2 Hz
Voice Coil Mirror	± 0.3 cm	5.86 μm[3]	60 Hz[2]
Piezo Mirror	$\pm 15\mu$m	0.6 nm	100 kHz

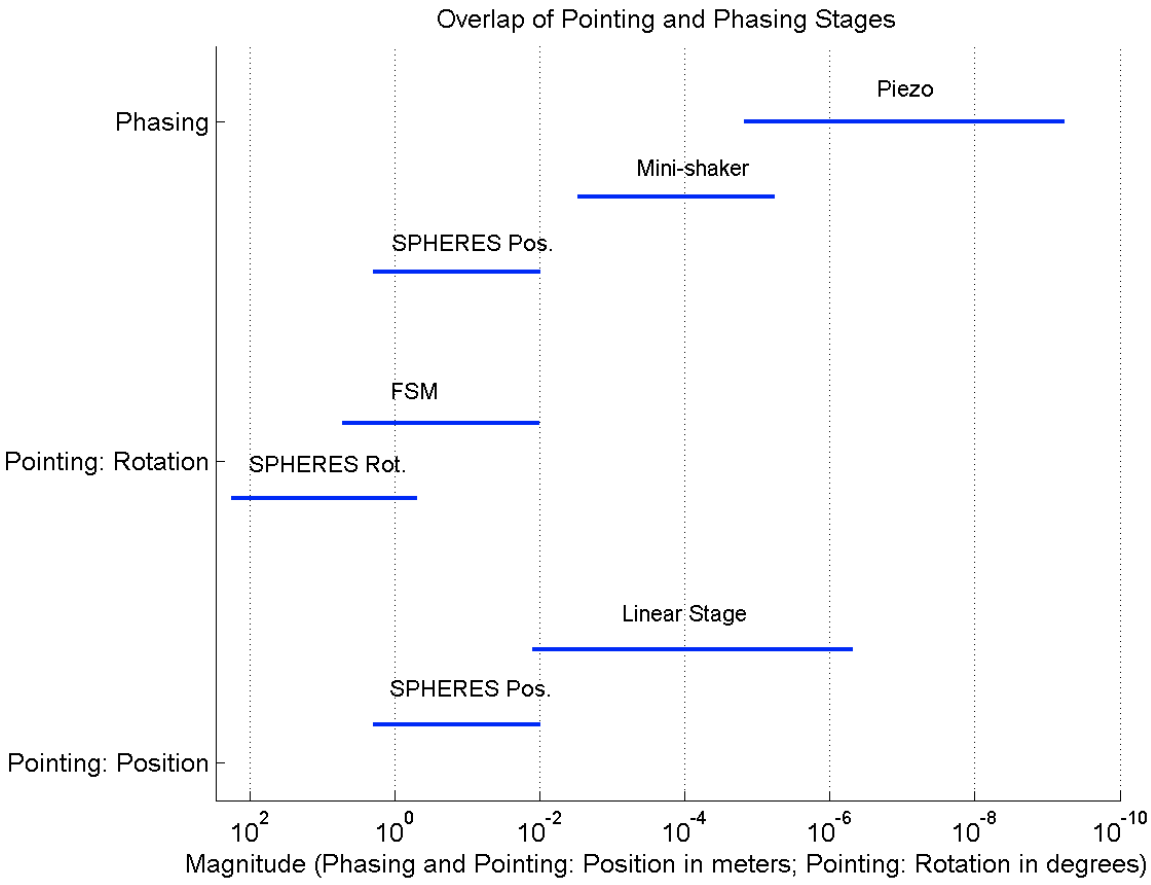

Figure 3-20: Overlap of pointing and phasing stages

3.6 Chapter Summary

This chapter discussed the setup for the SIMO testbed. It gave an overview of all of the components, how they interact with each other, and how they are used. It discussed how the components will be used to provide precise and accurate pointing control using the SPHERES satellite along with a linear stage and an FSM. This chapter also discussed the components that will be used for the phasing portion, and

[1]The bandwidth of the linear stage has not been determined. The stage is capable of moving at a speed of 1.02 cm/s, which is significantly faster than the satellite, resulting in adequate bandwidth.

[2]The bandwidth of a voice coil mirror is typically approximately 60 Hz. The actual value may vary for the FSM and Mini-shaker.

[3]Actual resolution will depend on system noise or DAC resolution. Figure assumes 10 bit DAC.

how an optical delay line will be used to achieve phasing. Chapter 4 discusses results from the initial validation of the testbed.

Chapter 4

Results

This chapter details the results from both formation acquisition tests as well as staged control tests. The formation acquisition tests were performed over two SPHERES Test Sessions onboard the International Space Station. The staged control tests were performed at the MIT Space Systems Laboratory.

4.1 Formation Acquisition

4.1.1 Pointing with Onboard Transmitter

The first tests performed using the SPHERES satellites only involved the satellites attempting to point their onboard beacons in the desired configuration. No relative positioning was attempted during these initial tests. The tests were first run on the SSL flat table, and then the tests were performed on the ISS during the SPHERES 18^{th} ISS Test Session. It was found during the tests that the onboard beacon did not perform as expected onboard the ISS. The field-of-view was expected to be approximately $60°$, but it was actually much larger. There were also issues with the beacon reflecting off surfaces, creating incorrect time of flight measurements. A simulated transmitter was used after these tests.

Three tests were attempted in increasing complexity to test the pointing portion of the formation acquisition. During all tests the satellites held their position in an equilateral triangular formation. The following tests were performed during Test Session 18:

1. All satellites begin with their transmitters pointing towards the center of the formation. (Figure 4-1)

2. One satellite points away from the center of the formation, while the other two point 55° away from the center of the formation. (Figure 4-2)

3. All satellites begin with their transmitters pointing away from the center of the formation. (Figure 4-3)

In the first test, the satellites began with all of their onboard beacon transmitters pointed towards the center of the formation, as seen in Figure 4-1. Unfortunately due to errors unrelated to the test, the satellites did not perform as expected. The subsequent tests did perform correctly, so the lack of results from this test was not a concern.

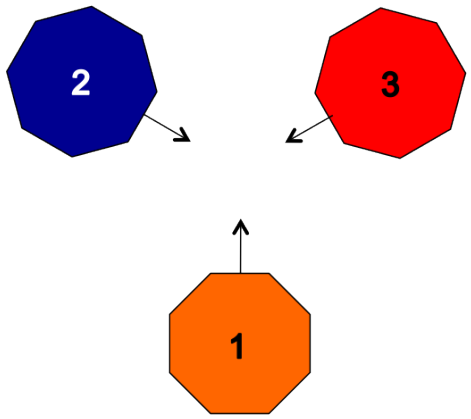

Figure 4-1: Initial positioning for first test

The second test began with satellite one pointed away from the center of the formation, and the other two satellites pointed towards each other, and away from

the center of the formation, as seen in Figure 4-2. In this test, satellite 1 should begin the pealing maneuver, as it should be outside of the range of the other satellites' beacons, and satellites 2 and 3 should point towards each other. However, satellite 1 was able to receive from satellite 2 and 3 immediately, before either satellite began rotating, and did not perform the pealing maneuver. The test was able to complete successfully, however. Satellite 1 became the primary satellite, satellite 2 became the secondary satellite, and satellite 3 became the tertiary satellite.

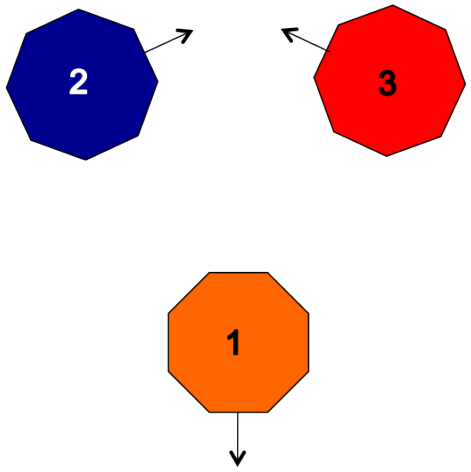

Figure 4-2: Initial positioning for second test

The third and final test run began with all satellites pointing their beacons away from the center of the formation, as seen in Figure 4-3. In this test, no satellites should be able to initially see the beacons of any of the other satellites, so all satellites should begin the pealing maneuver. However, satellite 1 was able to immediately see satellite 3's beacon. Satellite 1 then began to rotate towards satellite 3 after beginning relative state estimation. Two seconds later satellite 3 was able to see satellite 1's beacon as well, and began estimating relative states and rotating towards satellite 1. Satellite 2 was not able to initially see any other beacons, so it did begin the pealing maneuver. However, satellite 2 soon after saw satellite 1's beacon and began state estimation. The satellites successfully formed the desired formation, with satellite 1 as primary,

satellite 3 as secondary, and satellite 2 as tertiary.

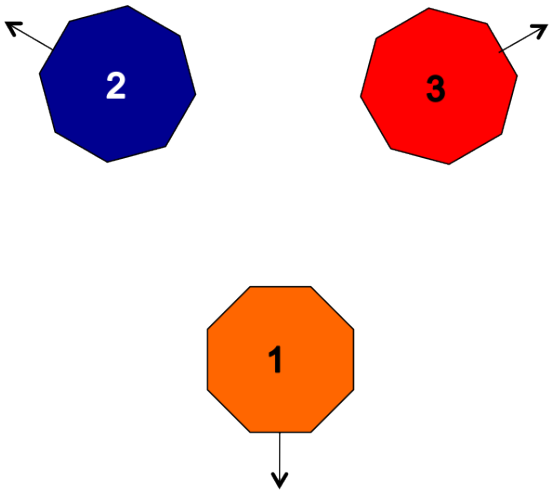

Figure 4-3: Initial positioning for third test

In summary, the satellites were able to use the relative estimates to successfully create the desired formation, but the characteristics of the onboard beacon limited the usefulness of the tests. The satellites did not need to use the pealing maneuver, as they were never truly "lost."

4.1.2 Simulated Beacon and Relative Positioning

After determining the issues with the onboard beacon, it was decided to use a simulated onboard beacon by having the satellites communicate their global states to each other and then calculating relative states when in view of another satellite's simulated beacon. This also made it possible to use the SPHERES MATLAB simulation to thoroughly test the algorithm before running tests on the SPHERES hardware. After running the simulations, five tests were run during the SPHERES 20$^{\text{th}}$ ISS Test Session. These tests included all four steps as described in Section 2.1 using the simulated onboard beacon. Table 4.1 summarizes the tests performed.

Table 4.1: Summary of tests performed during Test Session 20

Test	Initial Positioning	Initial Velocity
1	Triangular	Zero (holding position)
2	Triangular	Non-Zero
3	Triangular	Drifting
4	Linear	Drifting
5	Random	Drifting

Test 1

In the first test, the satellites begin with the global state vectors in Table 4.2. The satellites are in a non-equilateral triangular formation with their -X faces directed such that the other satellites are not within range of the field of view of the transmitters. A visualization of this formation can be seen in Figure 4-4. The black arrows on the satellites indicate the direction of the transmitter, which is located on the satellite's -X body axis.

Table 4.2: State vectors for satellites 1, 2, and 3 in test 1

	Satellite 1	Satellite 2	Satellite 3
POSX	-0.3	0.3	0.3
POSY	0	-0.4	0.4
POSZ	0	0	0
VELX	0	0	0
VELY	0	0	0
VELZ	0	0	0
QUAT1	0	-0.3314	-0.3314
QUAT2	0.3827	0.1913	-0.1913
QUAT3	0	0.8001	-0.8001
QUAT4	0.9239	0.4619	0.4619
RATEX	0	0	0
RATEY	0	0	0
RATEZ	0	0	0

The plots below show the results from the test, which was successful. The lines on the figures indicate what portion of the test the satellites are in, as described

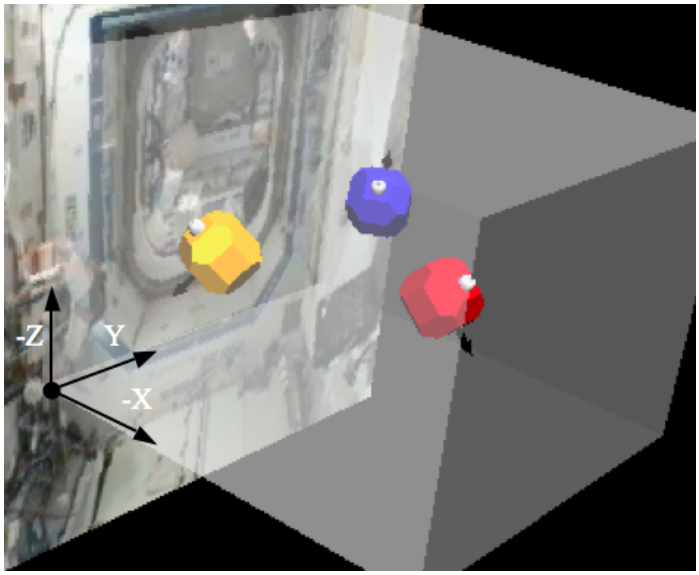

Figure 4-4: Visualization of the initial locations of the satellites

previously in Section 2.2. Figure 4-5 shows the separation between the satellites as the test progresses. During step 1, all satellites should have been holding position, but there was an error in the code, resulting in the satellites drifting. During steps 2 and 3, the satellites should again have been holding position, but they were instead trying to drive relative velocity to zero (this was not supposed to be done until later tests). During step 4 the satellites moved to their final desired positions, and the final separation was within approximately 3 cm of the desired 0.6 m separation between all satellites. The primary satellite should have been holding position during this step as well, but the error in the code allowed it to drift. The satellite did hold its position once the formation became too close to the boundary of the test volume at 92 seconds (an intended precautionary maneuver).

Figure 4-5 shows the pointing error for each satellite between its own transmitter and its desired final target. During step 1, all satellites performed the pealing maneuver. During step 2, all satellites pointed their beacon faces towards their partners: satellite 1 pointed towards satellite 2, satellite 2 pointed towards satellite 1, and satellite 3 pointed towards satellite 1. This indicates that satellite 1 was primary, satellite

2 was secondary, and satellite 3 was tertiary. During step 3, satellite 2 switched and pointed towards satellite 3, achieving the final desired configuration. The satellites continued to point to their desired targets during step 4, and the final error was less than 5 degrees.

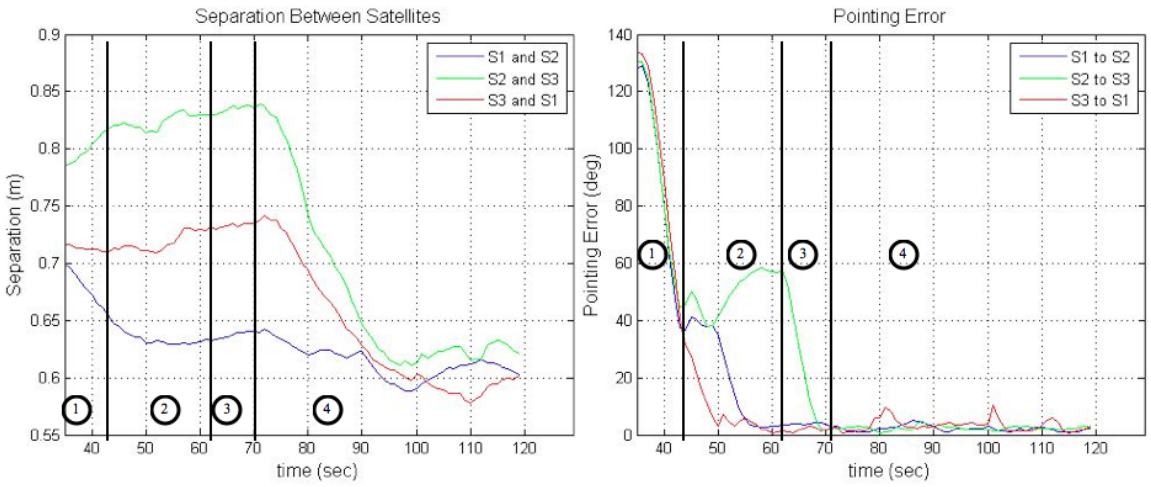

Figure 4-5: Distance between satellites (left) and pointing error between satellites (right) during test 1

Finally, Figure 4-6 shows the relative velocity between the satellites. During step 1 the satellites are attempted to hold position. During steps 2 and 3 the satellites tried to drive relative velocity to zero. During step 4 the satellites moved relative to each other to achieve the final desired formation, and then the relative velocity was low at the end of the test, as desired.

Test 2

This test began in the same configuration as the previous test, as seen in Figure 4-4, but two of the satellites began with some initial velocity. Satellite 1 (red) began with a velocity of 1 cm/s in the +X global direction, and satellite 2 (orange) began with a velocity of 1 cm/s in the +Z global direction. This test was run once and was successful; the satellites located each other and formed the desired formation.

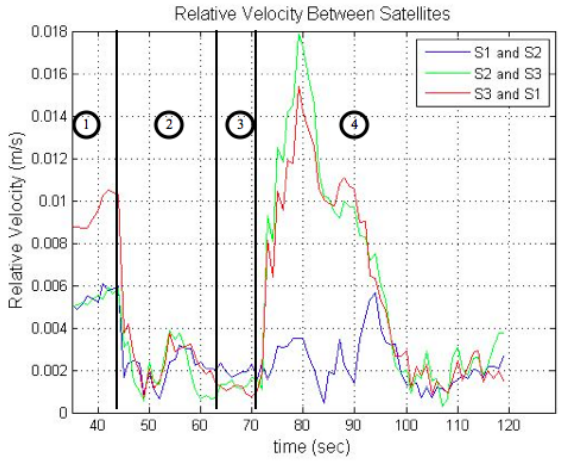

Figure 4-6: Relative velocity between satellites during test 1

The plots below show the results from the test. The lines indicate what portion of the test the satellites are in, as described previously. Figure 4-7 shows the separation between the satellites as the test progresses. During step 1, satellites 1 and 2 were travelling at their intended velocity, and satellite 3 was drifting. During steps 2 and 3, the satellites drove relative velocity to zero. During step 4 the satellites moved to their final desired positions, and the final separation was within 1 cm of the desired separation of 0.6 m.

Figure 4-7 shows the pointing error for each satellite between its own transmitter and its desired final target. During step 1, all satellites performed the pealing maneuver. During step 2, all satellites pointed their beacon faces at their partners: satellite 1 pointed towards satellite 2, satellite 2 pointed towards satellite 1, and satellite 3 pointed towards satellite 2. This indicates that satellite 2 was primary, satellite 1 was secondary, and satellite 3 was tertiary. During step 3, satellite 1 switched and pointed towards satellite 3, achieving the final desired configuration. The satellites continued to point to their desired targets during step 4, and the final error was less than 5 degrees.

Finally, Figure 4-8 shows the relative velocity between the satellites. During step

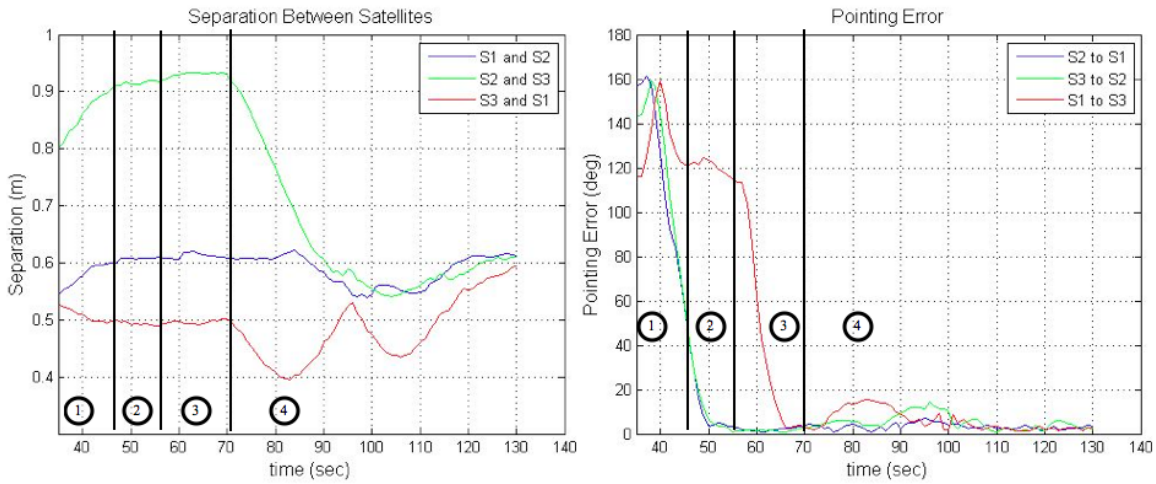

Figure 4-7: Distance between satellites (left) and pointing error between satellites (right) during test 2

1 the satellites were attempting to hold position. During steps 2 and 3 the satellites drove relative velocity to zero. During step 4 the satellites moved relative to each other to achieve the final desired formation, and then the relative velocity was low at the end of the test, as desired.

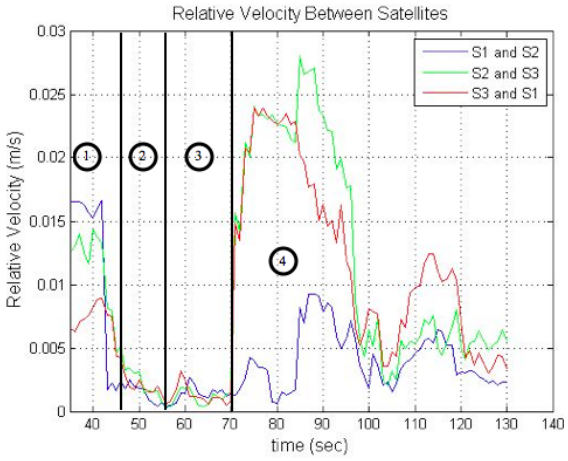

Figure 4-8: Relative velocity between satellites during test 2

Test 3

This test began in the same configuration as the previous two tests, as seen in Figure 4-4, but all satellites were allowed to drift in this test. This test was run once and was successful; the satellites located each other and formed the desired formation.

The plots below show the results from the test. The lines indicate what portion of the test the satellites are in, as described previously. Figure4-9 shows the separation between the satellites as the test progresses. During step 1, all satellites were drifting. During steps 2 and 3, the satellites attempted to drive relative velocity to zero, so relative position should be nearly constant. During step 4 the satellites moved to their final desired positions, and the final separation was approximately 0.6 m between all satellites at the end of the test, the desired configuration.

Figure 4-9 shows the pointing error for each satellite between its own transmitter and its desired final target. During step 1, all satellites performed the pealing maneuver. During step 2, all satellites pointed their beacon faces at their partners: satellite 1 pointed towards satellite 2, satellite 2 pointed towards satellite 1, and satellite 3 pointed towards satellite 1. This indicates that satellite 1 was primary, satellite 2 was secondary, and satellite 3 was tertiary. During step 3, satellite 2 switched and pointed towards satellite 3, achieving the final desired configuration. The satellites continued to point to their desired targets during step 4, and the final error was less than 5 degrees.

Finally, Figure 44 shows the relative velocity between the satellites. During step 1 the satellites were drifting. During steps 2 and 3 the satellites were trying to drive relative velocity to zero. During step 4 the satellites were moving relative to each other to achieve the final desired formation, and then the relative velocity was low at the end of the test, as desired.

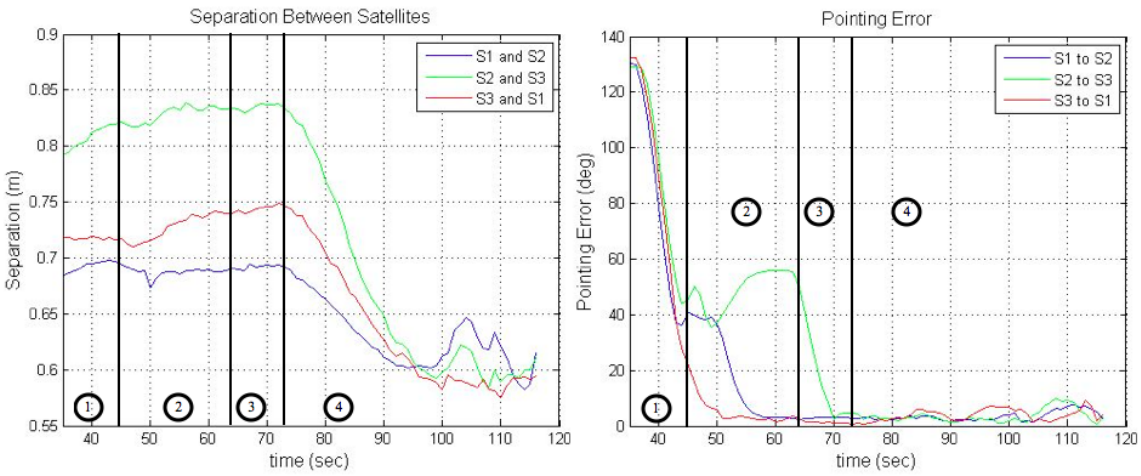

Figure 4-9: Distance between satellites (left) and pointing error between satellites (right) during test 3

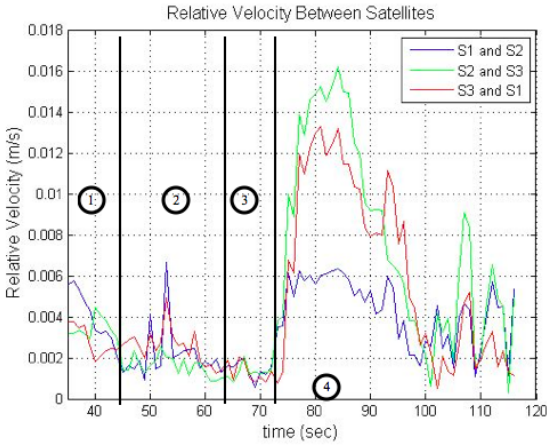

Figure 4-10: Relative velocity between satellites during test 3

Test 4

This test begins with all three satellites in a straight line, as seen in Figure 4-11. Table 4.3 shows the initial desired states of the three satellites. This configuration was chosen to add complexity to the test, and make it more difficult for the satellites to achieve the desired formation. The test was run once and was successful; the satellites achieved the desired final formation.

The plots below show the results from the test. The lines indicate what portion of

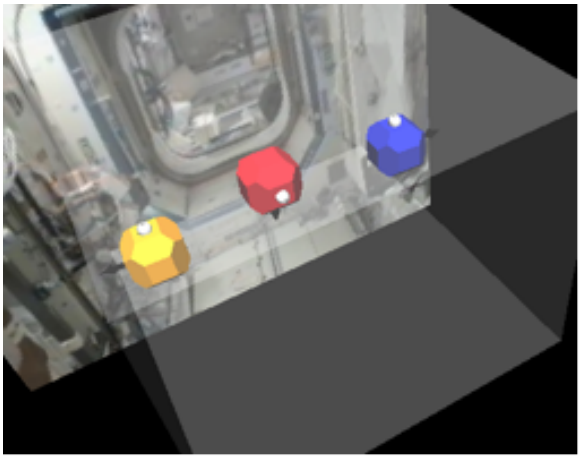

Figure 4-11: Satellite initial positioning for test 4

Table 4.3: State vectors for satellites 1, 2, and 3 in test 4

	Satellite 1	Satellite 2	Satellite 3
POSX	0	0	0
POSY	0	-0.5	0.5
POSZ	0	0	0
VELX	0	0	0
VELY	0	0	0
VELZ	0	0	0
QUAT1	0	0	0
QUAT2	0.707	0	0
QUAT3	0	0.707	-0.707
QUAT4	0.707	0.707	0.707
RATEX	0	0	0
RATEY	0	0	0
RATEZ	0	0	0

the test the satellites are in, as described previously. Figure 4-12 shows the separation between the satellites as the test progresses. During step 1 all satellites were drifting. During steps 2 and 3, the satellites attempted to drive relative velocity to zero, so relative position should be nearly constant. During step 4 the satellites moved towards their final desired positions. The distance between satellites 3 and 1 was larger than the other tests (0.68m instead of the desired 0.6m), but the relative velocity was small. If the requirements for position had been stricter, the relative position could

have been more accurate at the end of the test.

Figure 4-12 shows the pointing error for each satellite between its own transmitter and its desired final target. During step 1, all satellites performed the pealing maneuver. During step 2, all satellites pointed their beacon faces at their partners: satellite 1 pointed towards satellite 2, satellite 2 pointed towards satellite 1, and satellite 3 pointed towards satellite 1. This indicates that satellite 1 was primary, satellite 2 was secondary, and satellite 3 was tertiary. Since the satellites were in a line, the plot shows the error for satellite 2 is low during step 2. During step 3, satellite 2 switched and pointed towards satellite 3 (not much change is reflected in the plot, as satellite 2 is already pointing generally towards satellite 3), achieving the final desired configuration. The satellites continued to point to their desired targets during step 4. The final error was a bit higher than the other tests, due to the large amount of movement required to make the final formation. The error would have decreased if the requirements had been stricter. All satellites were pointing within approximately 20 degrees at the end of the test, which is still well within the field of view of the transmitter.

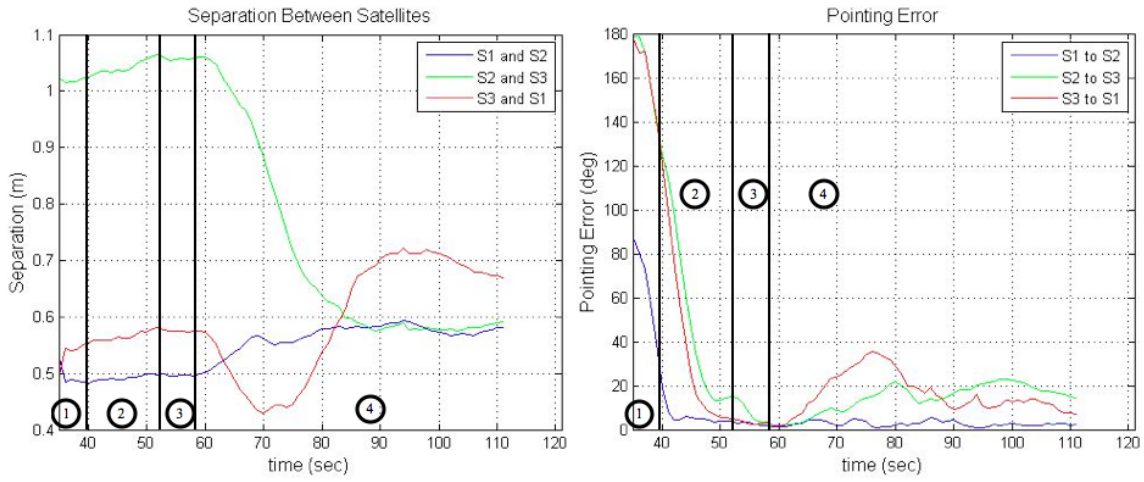

Figure 4-12: Distance between satellites (left) and pointing error between satellites (right) during test 4

Finally, Figure 4-13 shows the relative velocity between the satellites. During step

1 the satellites attempted to hold position. During steps 2 and 3 the satellites drove relative velocity to zero. During step 4 the satellites moved relative to each other to achieve the final desired formation, and then the relative velocity was low at the end of the test, as desired.

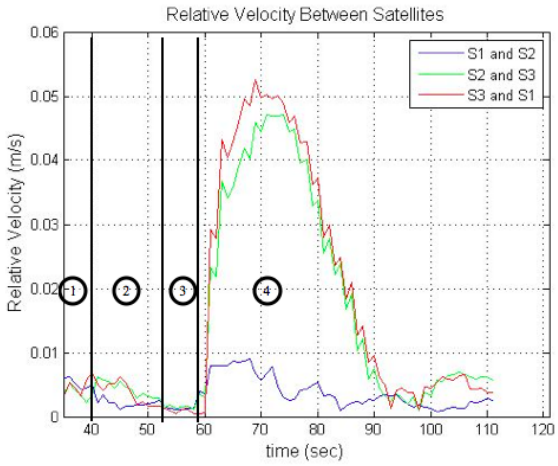

Figure 4-13: Relative velocity between satellites during test 4

Test 5

In this test, the astronaut randomly placed the satellites in the test volume. The formation acquisition began after a ten second estimation period. Figure 4-14 below shows the positioning of the satellites at the start of the test. Unfortunately the html document that instructs the astronaut on how to position the satellites was interpreted incorrectly and the astronaut placed the satellites with their beacon transmitters pointing towards each other, instead of away from each other. The test was attempted three times, but the test was only successful during the first attempt. During the two subsequent tests the astronaut correctly placed the satellites with their beacon transmitters facing away from each other, but the first test had two satellites reset, and there was a loss of communications in the third attempt. These errors were unrelated to the test. A fourth attempt was not made, as there was no time left allotted for

SPHERES science. The results from the first attempt, which was successful, are discussed below.

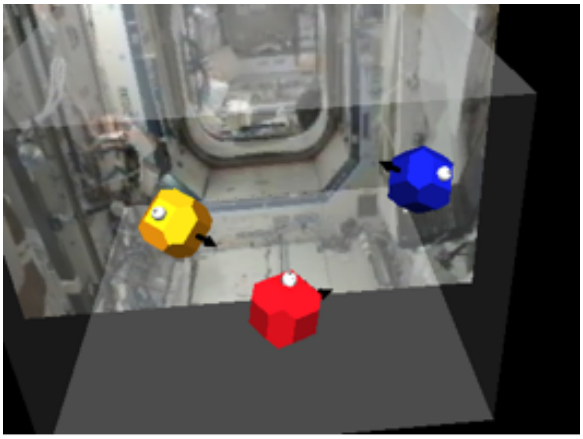

Figure 4-14: Satellite initial positioning for test 5

The plots below show the results from the test. The lines indicate what portion of the test the satellites are in, as described previously. Figure 4-15 shows the separation between the satellites as the test progresses. During step 1, all satellites were drifting. During steps 2 and 3, the satellites attempted to drive relative velocity to zero, so relative position should be nearly constant. During step 4 the satellites moved towards their final desired positions, and finished the test within 4 cm of the goal of 0.6 m.

Figure 4-15 shows the pointing error for each satellite between its own transmitter and its desired final target. During step 1, all satellites performed the pealing maneuver. Since the satellites begin with their beacon faces pointing towards each other, the peal was not necessary and the satellites immediately moved on to the next step. During step 2, all satellites were attempting to point their beacon faces at their partners: satellite 1 towards satellite 2, satellite 2 towards satellite 1, and satellite 3 towards satellite 1. This indicates that satellite 1 was primary, satellite 2 was secondary, and satellite 3 was tertiary. During step 3, satellite 2 switched and pointed towards satellite 3, achieving the final desired configuration. The satellites continued to point to their desired targets during step 4, and the final error was less

than 10 degrees.

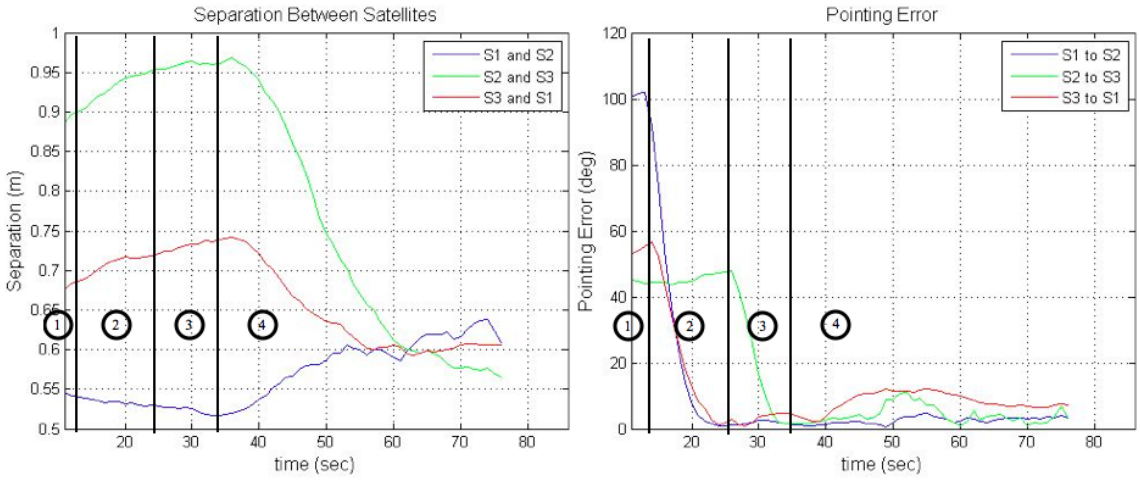

Figure 4-15: Distance between satellites (left) and pointing error between satellites (right) during test 5

Finally, Figure 4-16 shows the relative velocity between the satellites. During step 1 the satellites were drifting. During steps 2 and 3 the satellites attempted to drive relative velocity to zero. During step 4 the satellites moved relative to each other to achieve the final desired formation, and then the relative velocity was low at the end of the test, as desired.

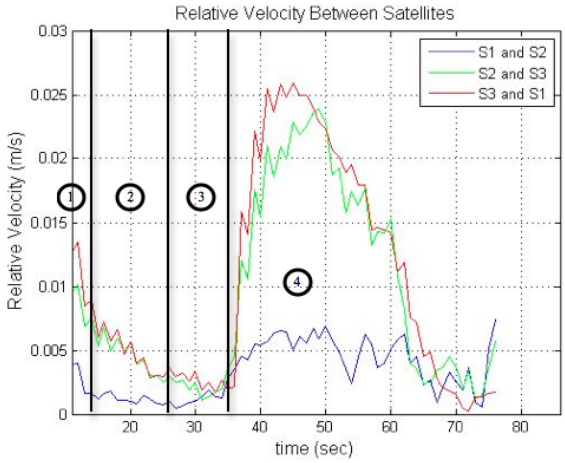

Figure 4-16: Relative velocity between satellites during test 5

4.2 Staged Pointing

4.2.1 Testbed Setup

In order to validate the SIMO testbed, a prototype for the testbed was developed on the MIT SSL flat table. The SPHERES satellites are capable of "floating" on the table using an air carriage powered by CO_2. Figure 4-17 shows the setup on the flat table in the MIT SSL. Included in this setup are the SPHERES satellite, the linear stage, the fast steering mirror, the camera for measuring pointing, the laser head, and the beam splitters. There are also electronics involved, including the PIC processor (which is attached to a PIC18 Explorer board), the digital to analog convertor, the mirror amplifiers, a TTL to RS-232 converter, and the linear stage controller. Figure 4-18 shows an overhead view of the laser, optics, and camera setup. Also visible is the screen attached to the power beam splitter.

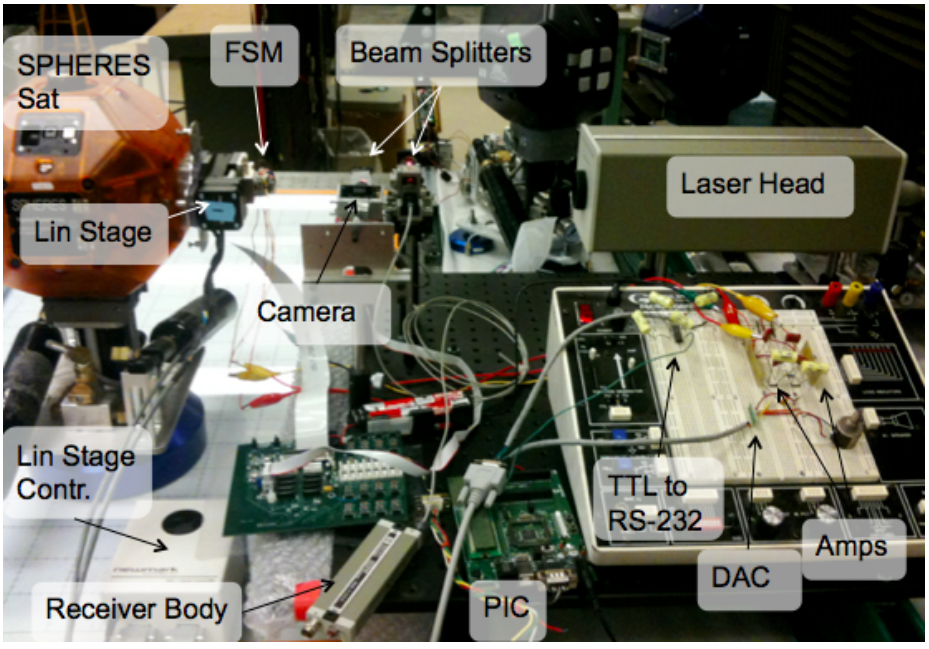

Figure 4-17: Initial setup for staged pointing tests

In this prototype, all of the electronics are off-board, so the satellite is tethered to the table. The satellite is still able to drift, but there are disturbances imparted

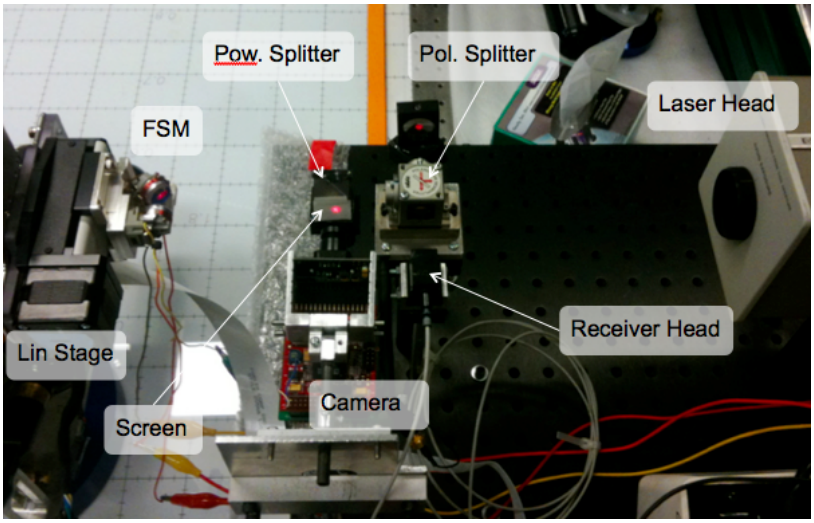

Figure 4-18: Overhead view of the setup for the staged pointing tests

by the wires that connect the satellite to the electronics. In the final testbed, the electronics will all be on a single board attached to the satellite at the expansion port.

Also in this setup, the external stack is not used for communicating with the camera. Instead, the camera communicates directly with the satellite. In the final testbed, this will not be possible, as it would require a cable to connect the camera to the satellite. However, since a cable was already necessary to connect the satellite to the off-board electronics, the camera was connected directly to the satellite for simplicity.

4.2.2 Fine Pointing

The first test run was with the satellite and linear stage both fixed and the FSM using integral control based off of measurements from the camera. The control period for this test is 0.5 seconds. Figure 4-19a shows the results from that test. The FSM is given a reference centroid to point at: (320, 240), which is the center of the CCD. Two disturbances were introduced at 34 and 53 seconds in the form of physically rotating the satellite to demonstrate the response of the mirror system. The plot

shows the error in position (measured in pixels) for both the vertical and horizontal axes. The mirror is able to quickly respond to the disturbances and return to the reference centroid within approximately 5 seconds. Figure 4-19b shows a close up of the error in both the horizontal and vertical axes. The resolution of the FSM is show to be approximately ± 1 pixel.

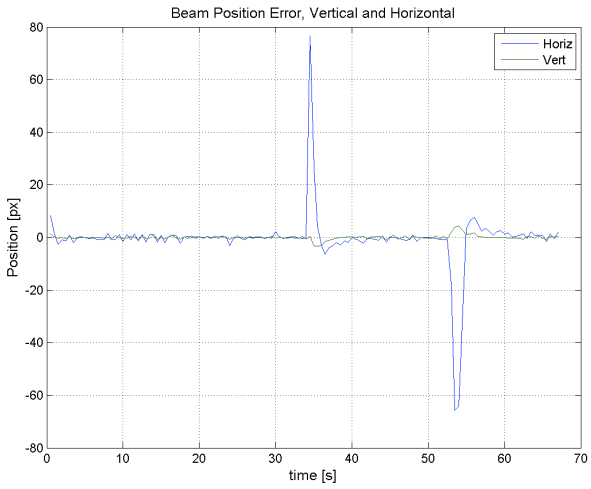

(a) FSM pointing error

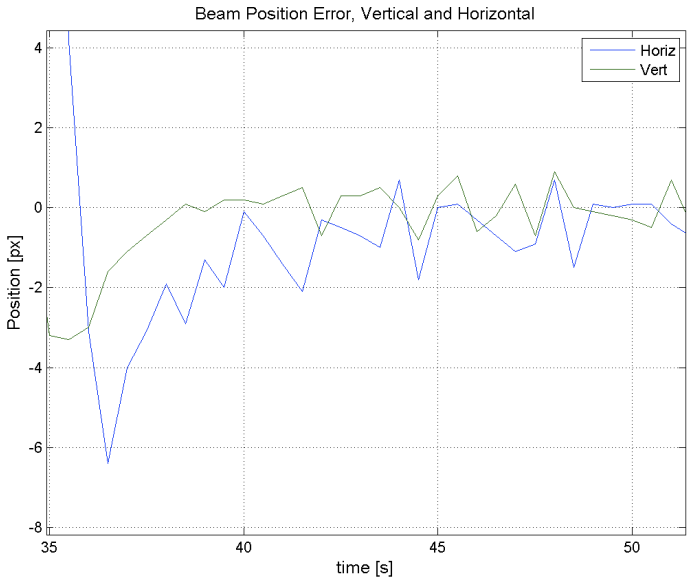

(b) Zoom in of FSM pointing error

Figure 4-19: Error in the positioning of the beam during fine pointing, measured by the camera

4.2.3 Fine Pointing with Estimation

In the second test, the satellite is still fixed, but it now runs the SPHERES estimator to determine its position and attitude. The FSM and linear stage use this information to determine how to move until the camera finds the centroid, at which point the FSM uses the data from the camera to point accurately. During the test, the satellite was physically moved and rotated to allow the linear stage and FSM to respond to changes in the state. Figure 4-20a shows the error in position of the satellite during the test from the reference position (the position the satellite would be in for the laser beam to hit the FSM with the linear stage centered). Figure 4-20b shows the error in rotation from the reference attitude during the test.

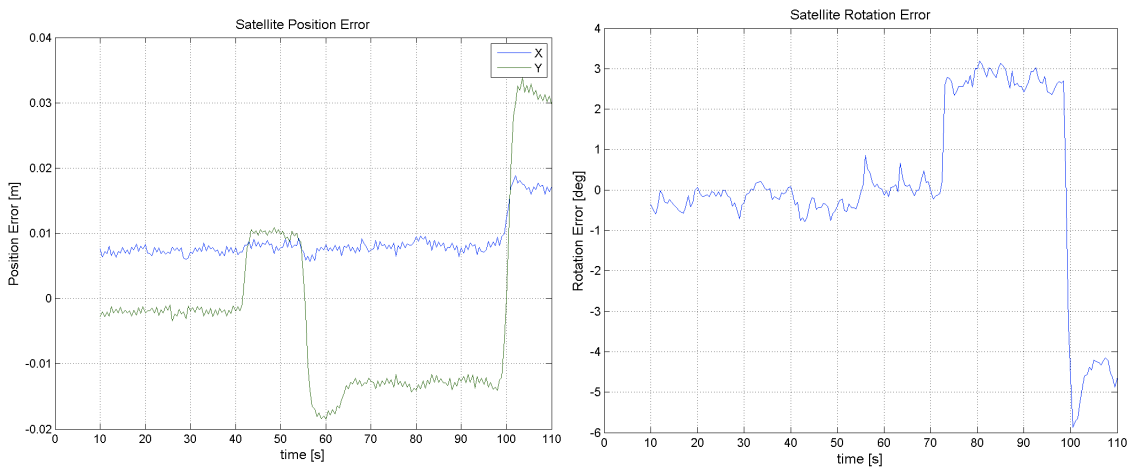

(a) Position (b) Roation

Figure 4-20: Error in position and rotation of the satellite during fine pointing with estimation

When the satellite was moved and rotated, the beam was no longer hitting the FSM, so the linear stage had to compensate for the errors. Figure 4-21 shows the error in the position of the beam during the test. When the beam falls off the FSM the camera can no longer see the beam, resulting in the drops off the plot seen in the figure. The short drop off at 42 seconds is due to the movement of the satellite in

the +Y direction, and the system is able to recover within approximately 2 seconds. The drop off at 54 seconds is due to movement in the -Y direction. This drop off is longer because the satellite was moved much further, so it takes longer for the linear stage to recover. There are also drop offs at 72 and 99 seconds due to a change in the satellite's rotation.

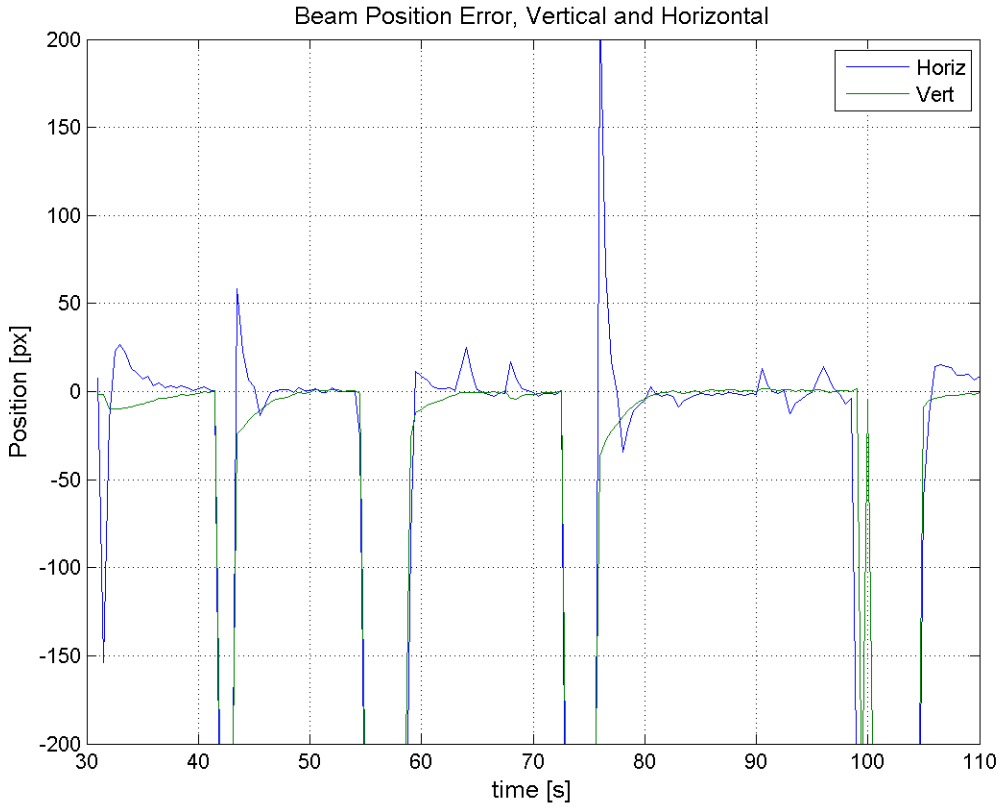

Figure 4-21: Error in the position of the beam during fine pointing with estimation, measured by the camera

4.2.4 Staged Pointing

The final pointing test was to have the satellite floating on the air carriage with the linear stage and FSM compensating for errors. The satellite first travels to its desired position. Once in position, the linear stage compensates for errors in position and

rotation. Then, the FSM compensates for errors in rotation. Once the beam can be seen by the camera the FSM can use the camera data to point.

Figure 4-22a shows the error in the satellite's position, and Figure 4-22b shows error in rotation. The satellite is unable to completely correct for the position error as there was a constant disturbance in the form of the connection between the satellite and the off-board electronics. The linear stage was able to compensate for these errors.

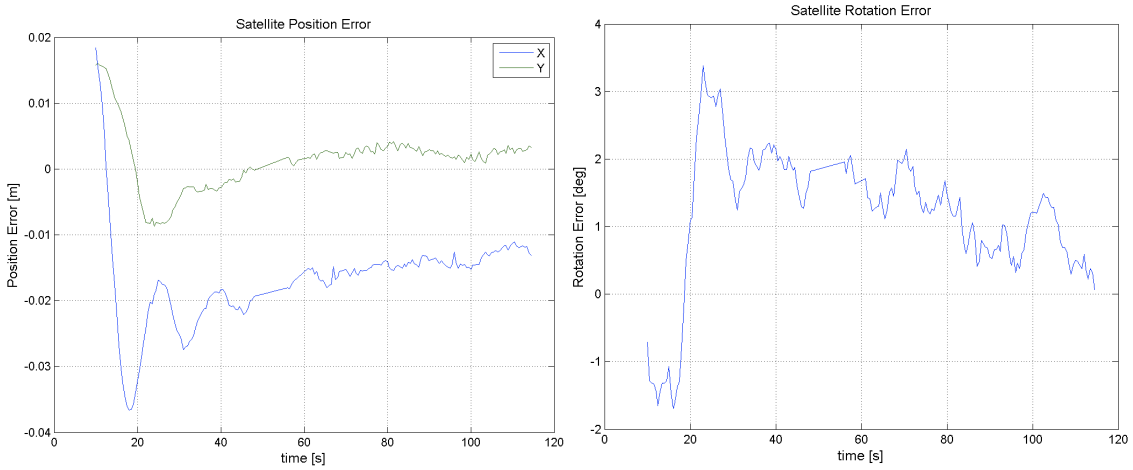

(a) Position (b) Roation

Figure 4-22: Error in position and rotation of the satellite during staged pointing

Figure 4-23 shows the error in the position of the beam during the test. The system is capable of approximately ±10 px control during the best portions of the test. At worst the system is capable of ±20 px control.

4.2.5 Resolution of the Staged Pointing System

In the prototype testbed, the satellite is placed such that the path length from the satellite to the screen that the camera images is 12 cm. The beam splitter is 2 cm wide, and the screen is placed directly in front of the splitter, so the screen width is also 2 cm. The lens of the camera is then places 1.3 cm from the screen. At this distance,

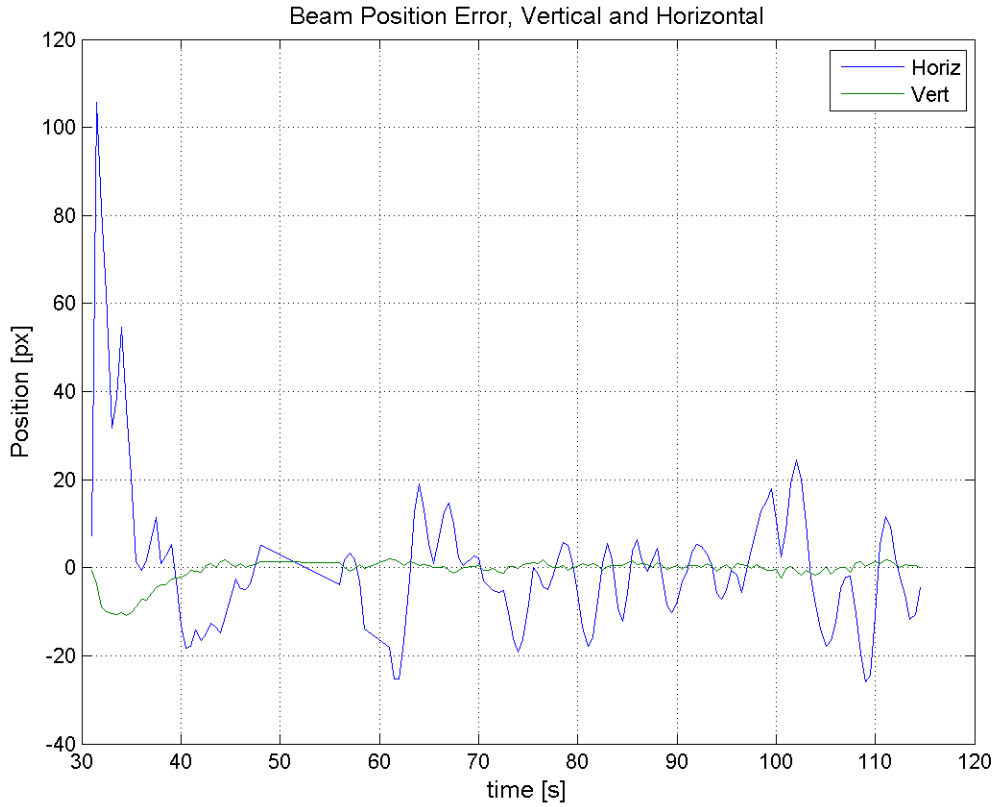

Figure 4-23: Error in the position of the beam during staged pointing, measured by the camera

the 2 cm screen takes up 492.3 pixels on the camera and the 6 mm beam takes up 147.7 pixels. So, a movement of 1 pixel on the camera corresponds to a movement of 0.00406 cm on the screen. At a distance of 12 cm, this corresponds to a change in angle of 0.0194°. Since the FSM changes the angle of the beam twice what it moves, this corresponds to a change in the FSM of 0.0097°, which is nearly the resolution of the FSM determined in Section 3.3.4 (0.0104°), and meets the requirements.

With the satellite floating, the precision of the system is reduced. Further controller development will increase the precision to the desired value. In its current state, the floating system is capable of controlling the position of the laser beam to approximately 0.194°.

4.3 Phasing

The phasing portion of the SIMO testbed has been designed, but not fully assembled or tested. The sensing system is currently capable of measuring path length using the Agilent receiver and PCI board. Neither of the stages has yet been connected to the computer or placed in the beam path. Figure 4-24 shows measurements from the interferometry system for a static test, in which the beam reflected off of the FSM while attached to the satellite. This resulted in a large amount of variation in the path length measured by the receiver. The reason for this variation is most likely vibration in the FSM (as it is a voice coil mirror). There is also likely vibration in the optics due to ground and building vibrations. These variations will need to be accounted for in the control of the phasing system.

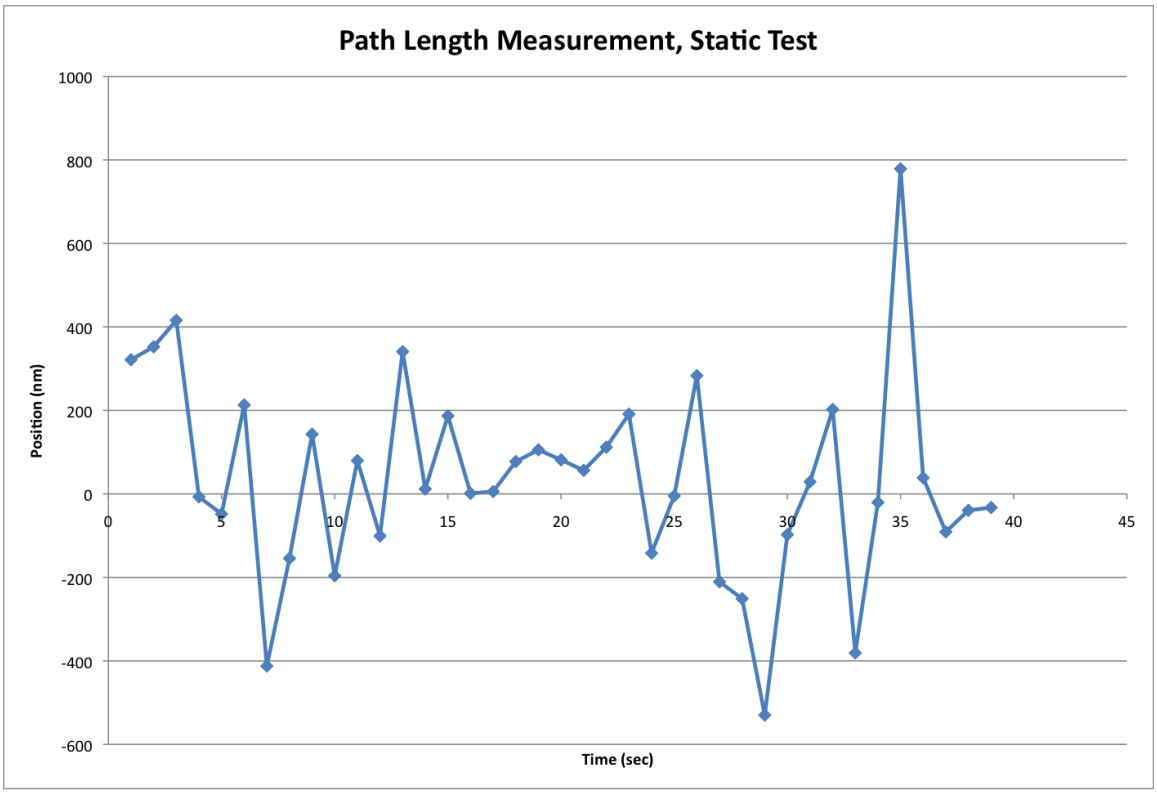

Figure 4-24: Path length (in nm) measured by the interferometry system

4.4 Chapter Summary

This chapter detailed results from formation acquisition tests and validation of the SIMO testbed. The initial formation acquisition tests had issues with the onboard beacon transmitter, which were fixed by using a simulated transmitter in the second set of tests. This second set of tests validated the algorithm. The SIMO staged pointing tests were also successful, and will be used to continue the development of the testbed. The phasing portion of SIMO has undergone initial testing, but there are still more tests to run to complete the testbed.

Chapter 5

Conclusion

5.1 Thesis Summary

Two different concepts related to formation flying interferometers are presented in this thesis. Chapter 2 presented an algorithm for initializing a formation of three satellites using relative sensors with limited fields-of-view. Chapter 3 presented a design for a staged pointing and phasing testbed. Chapter 4 presented the results from testing the formation acquisition algorithm and validating the SIMO staged control testbed.

The formation acquisition algorithm discussed in Chapter 2 builds off the work performed on two satellites at MIT [16]. The satellites begin by performing a three dimensional search. Each satellite continues to search until its limited field-of-view transmitter can be seen by another satellite, or until another satellite sees its transmitter. Once they detect each other, the satellites point their transmitters at each other, and then adjust so that each satellite is pointing at another satellite, and so no satellites are pointing at each other. After the pointing portion is completed, the satellites use relative range information, as well as global attitude data, to form an equilateral triangle.

Several tests were run to validate the formation acquisition algorithm. Section

4.1.1 describes the results from the first set of tests, which used the SPHERES onboard transmitter. These tests were not fully successful, as the satellites were able to detect each other without needing to perform a search. Section 4.1.2 describes the results from the second set of tests. These tests used a simulated transmitter, which worked by having the satellites communicate their global states to each other and then determine the relative states when appropriate. These tests were successful in validating the algorithm.

Chapter 3 discusses the development of the SIMO testbed. The goal of the testbed is to develop staged pointing and phasing by combining the coarse control of the SPHERES satellites with fine pointing and phasing actuators, creating an interferometer. The chapter describes all of the components involved, how they interact with each other, and how they will be used in the testbed.

The results from the initial tests of the pointing portion of the testbed are presented in Section 4.2. The results show that the pointing system has the ability to point accurately enough for the interferometer, but work still needs to be done to improve the controller while the satellite is floating. Section 4.3 presents the results from the initial phasing tests. No phasing control has been performed yet, but they sensing system is in place and has been proven to have the required precision.

5.2 Evaluation of Objectives

This thesis was successful in developing an algorithm for the initialization of a three satellite formation. The algorithm was also successfully tested on the SPHERES hardware, completing one of the objectives for this thesis. The algorithm is specific to satellites that have a limited field-of-view transmitter, omnidirectional receivers, and omnidirectional communication. The method may be applicable for other sensor configurations as well, and further work could be performed to investigate this.

This thesis was also successful in developing a design for a staged pointing and phasing testbed. However, this testbed still must be developed further to complete the design and verification. Without complete verification of the testbed the second objective was not fully met, but it should be possible to build on the concepts in this thesis to complete the testbed. The pointing portion of the testbed was confirmed to have the ability to meet the objectives of the SIMO project, but the control needs to be improved to achieve the required precision while the satellite is floating. The initial steps for the phasing system are in place, but still need to be tested. Control algorithms need to be developed as well for the optical delay line to control the path length of the beam to the desired precision.

5.3 Contributions

This thesis made the following contributions:

- An algorithm for the initialization of a three satellite formation.
- A framework for using a simulated sensor with the SPHERES satellites.
- Results from testing three satellite formation initialization on hardware, using limited field-of-view sensors.
- The design of a staged pointing and phasing testbed.
- Validation of the staged pointing system used in the SIMO testbed.
- Precision staged pointing control using the SPHERES satellites as coarse control and a fast steering mirror and linear stage as the fine control. The precision of the system is on the order of 0.02° when the satellite is stationary and 0.19° when the satellite is floating.

- Validation of the sensing system used for staged phasing control in the SIMO testbed.

5.4 Recommendations for Future Work

5.4.1 Formation Acquisition

While this thesis did succeed in developing an algorithm for initializing a three-satellite formation, there is room for further development. First, during the ranging portion of the algorithm, two of the satellites move relative to the Primary satellite. This maneuver results in unbalanced fuel consumption by the three satellites. If fuel balancing is desired, the three satellites could instead move together about the center of the formation, distributing the necessary fuel to complete the formation between them.

While there are proposed missions that have just three satellites in formation, there are also missions that plan to have many much larger formations. There should be investigation into how this algorithm could be used to initialize a larger formation.

By using a simulated sensor it becomes relatively simple to alter the transmitter/receiver configuration. Tests could be run with different transmitter field-of-views, and the transmitter could be moved to a different face. It would also be interesting to make a limited field-of-view receiver, which could be more representative of an actual satellite. In this case, the satellites would have to point their transmitters and receivers at each other at the same time in order to determine relative states, making a more difficult search. Communication could also be limited to a specified field of view, simulating a directional antenna.

5.4.2 Staged Pointing and Phasing

This thesis provides the design of a staged pointing and phasing testbed, but does not validate the completed testbed. One of the first steps will be to complete the pointing payload, with all of the electronics onboard the satellite. Once the electronics are onboard, it will be possible to move the satellite to the desired test distance from the optics, as well as test different test distances. A more robust and advanced controller for the pointing system should be developed as well, taking into account the current rotation of the satellite when controlling the mirror, instead of only using the camera data.

The phasing subsystem also should be validated. The first step will be to determine the best way to output data to the voice coil and piezo mirrors. This will most likely be through a digital to analog converter board, such as National Instrument's PCI-6221 Data Acquisition PCI board, which is able to interface with MATLAB. The phasing system can then be validated using a static path.

Once the phasing control system has been finalized, the pointing and phasing systems will be integrated. The desired final test is to have two satellites floating on air carriages with the optical delay line providing phasing control using feedback from the interferometry sensor.

Bibliography

[1] Agilent Technologies. *Laser and Optics User's Manual*, 2002.

[2] Aurora Flight Sciences. SIMO Phase 2 Proposal. NASA SBIR Proposal, Aurora Flight Sciences, July 2008.

[3] Brüel & Kjær. Mini-shaker - Type 4810. Data Sheet, January 2008.

[4] Kenneth G. Carpenter, et al. Stellar Imager Final Report Executive Summary. Mission Study, NASA, September 2005.

[5] M. Mark Colavita and Peter L. Wizinowi. Keck Interferometer: progress report. In *SPIE Optics and Photonics*, Munich, Germany, March 2000.

[6] ESA. FAQ. `http://www.spacetelescope.org/about/faq/`.

[7] Robert L. Grogan, Gary H. Blackwood, and Robert J. Calvet. Optical Delay Line Nanometer Level Pathlength Control Law Design For Space-Based Interferometry. In *SPIE Int. Symposium on Astronomical Interferometry*, April 1998.

[8] Fred Y. Hadaegh, Daniel P. Scharf, and Scott R. Ploen. Initialization of Distributed Spacecraft for Precision Formation Flying. In *IEEE Conference on Control Applications*, Istanbul, Turkey, June 23-25, 2003.

[9] John J. Hench, Boris Lurie, Robert Grogan, and Richard Johnson. Implementation of nonlinear control laws for an optical delay line. In *IEEE Aerospace Conference*, March 2000.

[10] JPL. SIM: What is SIM Lite? `http://planetquest.jpl.nasa.gov/SIM/whatIsSIM/`.

[11] Edmund M. Kong, Alvar Saenz-Otero, Simon Nolet, Dustin S. Berkovitz, and David W. Miller. SPHERES as a Formation Flight Algorithm Development and Validation Testbed: Current Progress and Beyond. In *2nd International Symposium on Formation Flying Missions and Technologies*, Washington, D.C., Sep. 14-16, 2004.

[12] Ryan Lim. Staged Attitude-Metrology Pointing Control and Parametric Integrated Modeling for Space-based Optical Systems. Master's Thesis, MIT, Aerospace Engineering, May 2006.

[13] Kuo-Chia (Alice) Liu. *Stochastic Performance Analysis and Staged Control System Designs for Space Based Interferometers*. PhD Thesis, MIT, May 2003.

[14] Boris Luire, John J. Hench, Asif Ahmed, and Fred Y. Hadaegh. Nonlinear Control of the Optical Delay Line Pathlength. In *SPIE*, Orlando, FL, April 1999.

[15] Richard G. Lyon, Kenneth G. Carpenter, Alice Liu, Peter Petrone, Peter Dogoda, Daniel Reed, and David Mozurkewich. Wavefront Sensing and Closed-Loop Control for the Fizeau Interferometry Testbed. In *SPIE Optics and Photonics*, San Diego, CA, Aug 26-30, 2007.

[16] Christophe P. Mandy, Hiraku Sakamoto, Alvar Saenz-Otero, and David W. Miller. Implementation of Satellite Formation Flight Algorithms Using SPHERES aboard the International Space Station. In *International Symposium on Space Flight Dynamics*, Annapolis, MD, Sept 24-28 2007.

[17] MIT SSL. MIT Space Systems Lab. `http://ssl.mit.edu/research/current.html`, 2009.

[18] Swati Mohan, Hiraku Sakamoto, and David W. Miller. Formation control and reconfiguration through synthetic imaging formation flying testbed (SIFFT). In *SPIE Optics and Photonics*, San Diego, CA, Aug 26-30, 2007.

[19] NASA. LISA - Laser Interferometer Space Antenna. `http://lisa.nasa.gov/`.

[20] NASA. Planet Quest: Missions - Terrestrial Planet Finder. `http://planetquest.jpl.nasa.gov/TPF/tpf_what_is.cfm`.

[21] NASA. The James Webb Space Telescope - FAQ. `http://www.jwst.nasa.gov/faq.html`.

[22] National Semiconductor. LM4861 Boomer Datasheet, February 2003.

[23] Newmark Systems. Microslide Linear Stage. `http://www.newmarksystems.com/downloads/PDF/Microslide.pdf`, 2003.

[24] OmniVision Technologies, Inc. OV9655/OV9155 Datasheet. `http://www.surveyor.com/blackfin/OV9655-datasheet.pdf`, November 2006.

[25] Joe Parrish. Synthetic Imaging Maneuver Optimization (SIMO) Quarterly Progress Report #1. NASA SBIR Phase II Quarterly Report, Aurora Flight Sciences, July 2009.

[26] Physik Instrumente. S-325 Piezo Z/Tip/Tilt Platform. Data Sheet, 2008.

[27] Andrew Robertson, Tobé Corazzini, and Jonathan P. How. Formation Sensing and Control Technologies For a Separated Spacecraft Interferometer. In *American Control Conference*, June 1998.

[28] Alvar Saenz-Otero. *Design Principles for the Development of Space Technology Maturation Laboratories Aboard the International Space Station.* PhD Thesis, MIT, May 2005.

[29] Daniel P. Scharf, Scott R. Ploen, Fred Y. Hadaegh, and Garett A. Sohl. Guaranteed Spatial Initialization of Distributed Spacecraft Formations. In *AIAA Guidance, Navigation and Control Conference*, Providence, RI, Aug 16, 2004.

[30] Surveyor Corporation. Surveyor SRV-1 Blackfin Camera. `http://www.surveyor.com/blackfin/`, May 2010.